ULTRASONIC ATTENUATION IN SUPERCONDUCTING ALUMINIUM

R. DAVID

ULTRASONIC ATTENUATION IN SUPERCONDUCTING ALUMINIUM

PROEFSCHRIFT

TER VERKRIJGING VAN DE GRAAD VAN DOCTOR IN DE WISKUNDE EN NATUURWETENSCHAPPEN AAN DE RIJKSUNIVERSITEIT TE LEIDEN, OP GEZAG VAN DE RECTOR MAGNIFICUS DR. D. J. KUENEN, HOOGLERAAR IN DE FACULTEIT DER WISKUNDE EN NATUURWETENSCHAPPEN, TEN OVERSTAAN VAN EEN COMMISSIE UIT DE SENAAT TE VERDEDIGEN OP WOENSDAG 21 OKTOBER 1964 TE 14 UUR

DOOR

RUDOLF DAVID

GEBOREN TE LEIPZIG IN 1931

PROMOTOR: PROF. DR. N. J. POULIS

Aan mijn ouders

Aan Bea

δός μοι ποῦ στῶ καὶ κινῶ τὴν γῆν.

Archimedes

Teneinde te voldoen aan de wens van de Faculteit der Wiskunde en Natuurwetenschappen geef ik hier een kort overzicht van mijn universitaire studie.

Nadat ik in 1950 mijn eindexamen had behaald aan het Stedelijk Gymnasium te Leiden begon ik de studie in de wis- en natuurkunde aan de Rijksuniversiteit te Leiden. Het eerste gedeelte van de studie moest gedurende twee jaar worden onderbroken in verband met militaire dienst.

Na het behalen van het candidaatsexamen letter A in 1955 begon ik als leerling van Prof. Dr. A. F. van Itterbeek mijn opleiding aan het Kamerlingh Onneslaboratorium, waarbij ik Dr. A. M. R. van Iersel hielp bij het voorbereiden en in 1958, samen met Prof. Dr. E. W. Guptill uit Halifax, bij het uitvoeren van zijn metingen over absorptie van ultrageluid in mengsels van ^{3}He en ^{4}He. Voorts assisteerde ik van 1956 tot 1959 op het natuurkundig practicum. Tevens bracht ik in 1957 enige maanden door op het Instituut voor Lage Temperaturen en Technische Physica van de Leuvense universiteit.

In 1958 legde ik het doctoraal examen experimentele natuurkunde af. De tentamens in de theoretische natuurkunde en de mechanica werden mij afgenomen door Prof. Dr. S. R. de Groot, Prof. Dr. J. van Kranendonk en Prof. Dr. P. Mazur.

Na het behalen van het doctoraal examen werkte ik gedurende enige tijd aan het uitwerken van een methode om zeer nauwkeurig de absolute waarden van voortplantingssnelheden in vloeistoffen te bepalen met behulp van cylindrische bariumtitanaat transducenten. In mei en juni 1959 hield ik mij aan het Centre d'Etudes de Chimie Métallurgique van het CNRS te Vitry-sur-Seine bezig met zonesmelten en met het maken van eenkristallen van aluminium, onder leiding van Prof. Dr. F. Montariol.

In het najaar van 1959 begon ik aan het onderzoek waaruit dit proefschrift is voortgekomen. Ik trad toen in dienst van het Natuurkundig Laboratorium der N.V. Philips' Gloeilampenfabrieken, waarbij mij de gelegenheid werd geboden mijn onderzoek aan het Kamerlingh Onneslaboratorium uit te voeren. Ik ben de Directie van het Natuurkundig Laboratorium van Philips erkentelijk voor het treffen van deze voor mij zeer plezierige regeling.

Het onderzoek heeft deel uitgemaakt van het programma van de groep VS-L van de Stichting voor Fundamenteel Onderzoek der Materie, waartoe financiële steun is verleend door de Nederlandse Organisatie voor Zuiver Wetenschappelijk Onderzoek. Genoemde werkgroep staat onder leiding van

Prof. Dr. C. J. Gorter, die veel heeft bijgedragen tot de interpretatie van de meetresultaten. Bij het voorbereiden en uitvoeren van de metingen en bij het uitwerken van de resultaten ben ik geassisteerd door de heren Drs. T. Blangé, J. Dussel, H. R. van der Laan en J. Siegenbeek van Heukelom. Bij het bewerken van dit proefschrift zijn discussies met Dr. P. G. Klemens uit Pittsburgh voor mij zeer nuttig geweest.

Tijdens mijn werkzaamheden op het Kamerlingh Onneslaboratorium heb ik veel steun ondervonden van de zijde van de technische staf. Zonder anderen tekort te willen doen vermeld ik in het bijzonder de hulp van de heren P. Nachtegaal, H. R. Nater, Th. Nieboer en H. van Zanten. Zelfs waar het schijnbaar onoplosbare problemen betrof hebben zij mij steeds op prettige wijze met raad en daad bijgestaan.

Abstract

This thesis deals with the absorption of ultrasound in superconducting aluminium. The results of the measurements using longitudinal sound waves in specimens of different purity are in agreement with the theory of Bardeen, Cooper and Schrieffer. Extrapolation leads to a zero-temperature energy gap of $3{\cdot}5\,kT_c$. The absorption of transverse sound waves can be split up into two parts, namely one part according to the BCS theory, and one part which decreases rapidly below the superconducting transition temperature and is zero from 0·02 °K below the transition temperature. This second part of the absorption is also negligibly small when the product of the wave number of the sound and the mean free path of the electrons is much smaller than unity. This has been shown by experiments on specimens of different purity using sound of different frequencies. Measurements were performed on two single crystals of zone-refined aluminium with different sound-polarization directions. The value of the absorption depended on the polarization direction, but the calculated energy gap did not. Phase transitions in a very pure zone-refined aluminium single crystal were also investigated using ultrasound, in order to find out something about the propagation velocity of the phase boundaries, and the structure of the intermediate state. For the latter, measurements at different temperatures and different frequencies were required. The experimental results for magnetic fields both parallel and perpendicular to the sound-propagation direction support the theories of Pippard and Faber. During the transition from the superconducting to the normal phase the absorption behaves as predicted by Pippard on the basis of the eddy-current theory. A formal description is also given of the transition from the normal phase to the superconducting phase. In the very pure specimen used, thin normally conducting regions were found to exist for more than twenty minutes after an external magnetic field of the order of the critical field had been switched off. All transition times are much shorter for less pure aluminium.

CONTENTS

INTRODUCTION

Bömmel [54,1]) in 1954 was the first to measure ultrasonic attenuation as a function of temperature in a superconducting metal. Since then many investigations have been carried out in this field. Only few measurements have been reported on ultrasonic attenuation in aluminium [58,1]) [59,1]) [59,2]) [62,1]). One single paper [62,1]) refers to measurements on aluminium well below the transition temperature, which is about 1·16 °K. Complicated cryogenic problems connected with cooling of the specimens have undoubtedly limited the number of papers on this subject.

Experiments on ultrasonic attenuation in superconducting metals became of great interest when a theoretical description was developed on the basis of the theory of Bardeen, Cooper and Schrieffer [57,1]) which we shall call the "BCS theory" for short. This theory led to values of the absorption due to electron-phonon interaction in an isotropic metal in the superconducting state with respect to that when the metal is in the normal state.

In this thesis experiments are described that have been performed on pure and less pure specimens of aluminium by using both longitudinal and shear waves. The aim of the experiments was to compare the results with the BCS theory, to determine the energy gap for zero temperature and to look for orientation dependences. The normal-state attenuation was also measured as a function of the frequency. Furthermore, investigations at magnetic fields smaller than the zero-temperature critical field are reported.

In the last chapter ultrasonic attenuation measurements during phase transitions are described. Large differences were revealed between the results for magnetic fields parallel to the sound-propagation direction and for magnetic fields transverse to that direction. Some of the measurements were performed at different temperatures and at different frequencies. An expression for the transition velocity from the superconducting state to the normal state as a function of the external magnetic field is verified, and a tentative model for the structure of a specimen in the intermediate state is discussed on the basis of the measurements.

1. ON THE GENERAL THEORY OF ULTRASONIC ABSORPTION IN METALS

1.1. Phonons and electrons in metals

1.1.1. *Ultrasonic waves*

Sound in the ordinary sense is the name given to all those mechanical vibrations to which the human ear is sensitive. These mechanical vibrations are propagated through matter in the form of mechanical waves.

The frequency spectrum of mechanical waves in solids runs from the very lowest frequencies — corresponding to vibrations in which macroscopic regions move relatively to each other — to frequencies of the order of 10^{13} Hz, corresponding to the vibrations of individual atoms relative to their neighbours. The human ear is sensitive only to a small part of this frequency spectrum, from about 20 Hz to about 16 kHz. Sound of higher frequency is called ultrasound. In this thesis we shall sometimes refer to "ultrasonic waves" simply as "sound waves".

In a solid material there are two kinds of mechanical waves: those that can pass through the entire material, and those that are confined to surfaces or interfaces. The second kind, the surface waves, need not be considered in the present thesis, as in the experiments to be discussed the sound beam is generated in such a way that the beam does not strike any surface except at almost normal incidence.

With waves of the first kind, or body waves, we distinguish between waves of different polarizations. There are three independent modes of polarization, having three mutually perpendicular polarization directions. For propagation in an isotropic material, one of the modes is longitudinal, and the other two are transverse. The longitudinal wave is a compressional wave. The transverse waves give rise to deformations without change in volume; they are called shear waves. Even when this distinction is not sharp in practice, there will be, however, one wave predominantly compressional, which we call the longitudinal wave. All sound waves in a solid can be regarded as a superposition of waves of these three polarizations.

In order to study sound waves in a solid it is necessary to have a well-defined sound beam of a given frequency. This can be introduced into the solid by means of a transducer, which is placed at the surface of the specimen and converts electromagnetic waves into mechanical vibrations, a substantial fraction of which will be propagated through the solid. A transducer can also be used for the inverse process of converting part of the energy of a sound wave into electromagnetic waves, thus serving as a detector. Ideally the transducer should

generate only sound of one frequency for a given frequency of electromagnetic waves, and the sound waves emerging into the solid should have a narrowly defined propagation direction and only one polarization. These requirements can be approximated to by the arrangement which we shall be discussing in chapter 2. In common with widespread practice, quartz transducers are used here, as they have a wide frequency response, and their electromechanical properties show little temperature dependence. Besides, quartz is easily machined and has the additional advantage of being insoluble in most solvents.

The different interactions of stress waves with a given solid have been summarized by Truell and Elbaum [62,2]). Their introduction to the concepts of the theory of elasticity, in particular stress, strain and elastic constants, will not be repeated here. We only mention that stress energy can be dissipated in a body in many different ways, e.g. by interaction with conduction electrons in metals, by direct scattering by defects and by the thermoelastic effect.

Energy dissipation, to whatever mechanism it may be due, is commonly expressed in terms of an attenuation coefficient α, defined in the following way [63,1]). Assuming the decrease of the stress amplitude $|\sigma|$ over a small distance dx to be proportional to the stress amplitude itself and to the distance dx, one may write $d|\sigma| = -\alpha|\sigma|\,dx$. This expression may be integrated to give the stress amplitude at a distance x:

$$|\sigma| = \sigma_0 e^{-\alpha x}\,, \tag{1}$$

where σ_0 is the amplitude of the time-dependent stress at zero distance. The attenuation is therefore

$$\alpha = \frac{1}{x} \log_e \frac{|\sigma(x)|}{\sigma_0} \text{ neper/cm}\,, \tag{2}$$

if x is measured in cm.

In accordance with engineering practice it is convenient to give the attenuation coefficient as $20 \log_{10} |\sigma(x)|/\sigma_0$ in decibels/cm; α in decibels/cm is equal to 8·686 α in nepers/cm.

The experiments on ultrasonic attenuation which led to this thesis were performed by using the pulse technique described in chapter 2. High-frequency electric waves of about 1 μs duration from a pulsed oscillator were fed to a flat quartz plate which converted the electric energy into mechanical waves of the same frequency. The quartz plate reconverted reflected sound energy into electric waves. The high-frequency electric waves were transmitted to and from the transducer through coaxial cables. This pulse technique is useful for the frequency range from 1 to 300 MHz. Below 1 MHz the shape of the transducer makes it difficult to get a "monochromatic" sound beam, while at frequencies above 300 MHz electromagnetic losses in the equipment are predominant, so that wave guides are essential for transmitting the electromagnetic waves. At

radar frequencies electric energy is transmitted via a wave-guide system to a resonant cavity with a clamped transducer. Matching of the specimen to the transducer for performing measurements at these high frequencies still gives rise to difficulties.

1.1.2. *Thermal vibrations in solids*

The atoms in a solid vibrate about their equilibrium positions. Since the instantaneous equilibrium position of each atom depends upon the instantaneous position of its neighbours, the vibrations of all the atoms are interdependent. It is possible, however, to express the vibrations of a solid as a superposition of travelling elastic waves.

These waves, also called lattice waves, are described in the same way as the sound waves discussed in the previous section, except that they always cover a wide range of frequencies, from zero to around 10^{13} Hz, and a corresponding range of wavelengths from macroscopic dimensions down to the interatomic distance. At the shorter wavelengths, the consideration of an elastic solid as continuous must be replaced by considerations taking into explicit account the atomic structure of the material, and the relation between frequency and wavelength departs from the simple hyperbolic one which holds at lower frequencies. This effect is called dispersion.

At liquid-helium temperatures, as we shall see below, the predominant lattice waves have a wavelength of the order of 100 times the interatomic distance, and the dispersion of the lattice waves is unimportant.

The energy content of each wave is given by considerations of statistical mechanics, in complete analogy to the energy content of black-body electromagnetic radiation in an enclosure. In this connection it is important to note that the energy of each wave is quantized, and consists of an integral number of phonons, each of energy $h\nu$, where h is the Planck constant, and ν the frequency of the wave. The thermal energy is most concentrated at frequencies around $3kT/h$, where k is the Boltzmann constant and T the temperature. At 1 °K, this frequency is of the order of 30 GHz.

A typical plot of the number of phonons between ν and $\nu + d\nu$ against ν (a thermal spectrum or "Debye spectrum") is shown in figure 1, for 1 °K [58,2]). It is evident that the range of ultrasonic frequencies used in our experiments is restricted to the utmost left-hand part of the graph.

Although the frequencies obtained from conventional electronic equipment are always much lower than the central frequency of the Debye spectrum, measurements by means of ultrasonic waves in a solid can provide much information about properties of a solid. In principle the very-low-frequency waves available for ultrasonic experiments are also quantized, but the number of phonons there is always very large, and the results of quantum-mechanical

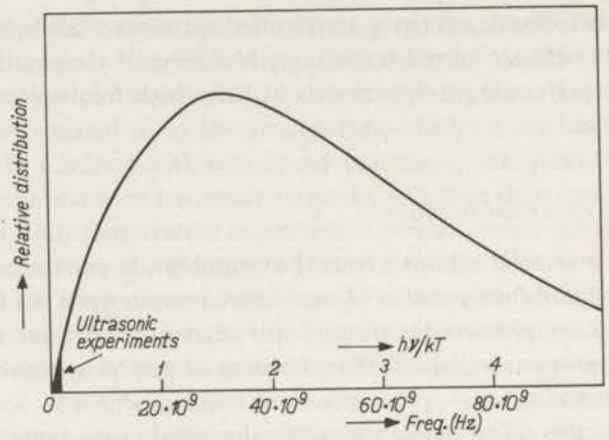

Fig. 1. The thermal spectrum of the lattice for $T = 1$ °K.

considerations coincide with the results of classical mechanics. Either approach can be used.

1.1.3. *Electrons in metals*

While in an insulating solid every electron is associated with a particular atom or atomic group, in metals some of the electrons, the conduction electrons, are free to move through the entire solid, and behave in many respects like a gas of free electrons. These conduction electrons are responsible for the characteristic properties of a metal: high electrical and thermal conductivity and high reflectivity.

The atoms of a solid metal are arranged in characteristic crystal lattice. A unit cell of the aluminium lattice is shown in figure 2. Aluminium has a face-centered cubic lattice structure.

In reality the crystal lattice is never perfect throughout the entire volume of a specimen. There are occasional lattice defects such as vacant sites, impurity

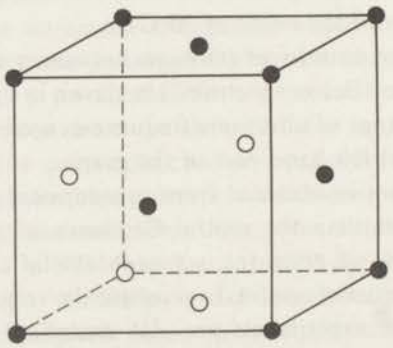

Fig. 2. Unit cell of aluminium showing face-centered-cubic lattice structure.

atoms and dislocations. In addition, metal specimens may be polycrystalline, that is they may consist of a large number of domains of different crystal orientation.

Although in a metal crystal each conduction electron is always in the close proximity of an atom, it follows from wave-mechanical principles that these electrons are not scattered when the atoms form a perfectly regular lattice. Scattering only occurs as a result of the departures of the lattice from perfect regularity, that is as a result of the various lattice defects, and the irregularity introduced into the lattice by the thermal motion of the atoms. This motion is best described by lattice waves.

The energy of the electron system is governed by the solution of a wave equation which takes into consideration the kinetic energy of the electrons and their potential energy under the influence of the electric fields produced by the atoms and by the other conduction electrons. To a good degree of approximation the total energy of the system is composed additively of the energies of the individual electrons, and the energy of each electron is some function of its momentum. The exact form of this function is very difficult to evaluate, and it is often convenient to replace this total energy by the energy of a free electron, using the mass of the electron as an adjustable parameter. The kinetic energy of such a quasi-free electron can be written in the following form

$$E_{\mathbf{k}} = \frac{\hbar^2 k^2}{2\, m^*}, \tag{3}$$

where $\mathbf{k}$ is the wave vector of that electron and m^* its effective mass.

The ground state of a whole system of free electrons is that where all energy levels are occupied up to a level which is called the Fermi energy, and no levels are occupied above this level. In $\mathbf{k}$-space the surface defined by the free electrons with Fermi energy, the Fermi surface, is a sphere. Putting the total number of electrons within the Fermi sphere equal to NV, where N is the number of electrons per unit volume and V the volume in ordinary space, one obtains the expression for the Fermi energy at $T = 0$ [60,1]) which will be used in chapter 3, viz.

$$E_F = \frac{\hbar^2}{2\, m^*} \left(\frac{3\, N}{8\, \pi}\right)^{2/3}. \tag{4}$$

At finite temperature the division between occupied and unoccupied states is not sharp, but spread out over an energy range of order kT. Formally this is described by attributing to every state an equilibrium-occupation probability given by the Fermi-Dirac distribution function $(e^{(E-E_F)/kT}+1)^{-1}$, where E_F is the Fermi energy.

Although it is known that the Fermi surface of real metals is not quite spherical, the spherical Fermi surface is a good first approximation for describing part of the properties of many metals, including aluminium [63,2]).

1.2. Absorption in normal metals at low temperatures

1.2.1. *Introduction*

The attenuation of a longitudinal ultrasonic wave due to the conduction electrons in a metal can be thought of as follows. Consider an element whose volume is small compared to the wavelength. This volume suffers a strain which is assumed to be uniform, and at the same time acquires a velocity. As a result there must be a current flow, partly to compensate the change in the material density, and partly due to the tendency of the electron gas to be at rest relatively to the motion of the lattice. The electron distribution takes a finite time to adjust itself to the changes in the density and velocity of each volume, so that the electronic motion is out of phase with the motion of the lattice. This leads to energy absorption, and since the time it takes for the electrons to adjust themselves to the lattice is also the relaxation time which governs the electrical conductivity, the absorption is related to the electrical conductivity, so that the value of the absorption is largest at lowest temperatures. It follows that the absorption increases to a limiting value as the temperature is decreased to very low values. This has been verified experimentally for several pure metals. When plotting the attenuation in pure metals at low temperatures as a function of temperature one obtains a picture similar to that in figure 3. In that figure the attenuation of longitudinal ultrasonic waves below 16 °K, as measured by Mason and Bömmel [56,1]), has been plotted against temperature for a normal-state tin single crystal.

The approach given above is justified as long as the wavelength of the sound is much longer than the mean free path of the electrons. In the extreme opposite case, one can think of the sound-wave interacting not with the electron gas as a

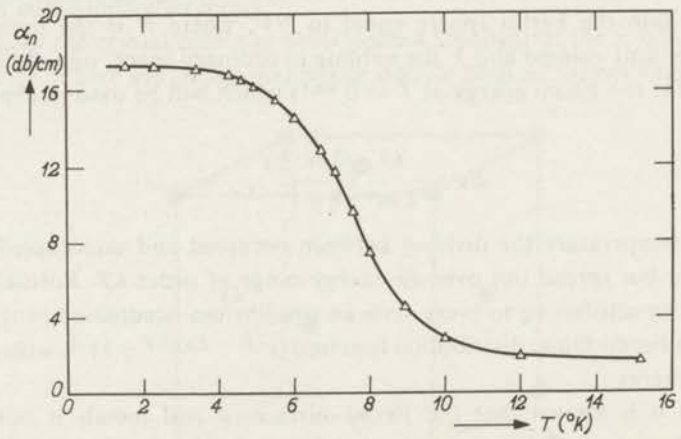

Fig. 3. Attenuation of longitudinal sound waves as a function of the temperature in a normal-state tin single crystal along the (001) axis, $\nu = 60$ MHz, after Mason and Bömmel.

whole, but with the individual electrons. This way of looking at the interaction is a consequence of Bloch's reasoning to obtain the various conduction properties; in particular Makinson obtained an expression for the attenuation coefficient for lattice waves and used it to deduce the lattice thermal conductivity. When the wavelength of the sound is much smaller than the mean free path of the electrons in a specimen, the absorption of sound waves is independent of the relaxation time of the electrons in the same specimen.

In the case of alloys, and in the case of metals at room temperature, the mean free path of the conduction electrons is short, typically of the order of 10^{-5} cm, and the absorption of ultrasonic waves is governed by the interaction with the electron gas as a whole; it is thus proportional to the conductivity. For pure metals the absorption increases when the temperature is reduced. If the frequency of the ultrasonic waves is high enough, and the metal sufficiently pure, one reaches a region below liquid-hydrogen temperatures where the absorption is given by the latter considerations, namely interaction with individual electrons; here the absorption is independent of the relaxation time, and also the frequency dependence for the ultrasonic absorption is changed.

The absorption of ultrasonic waves in normal metals at low temperatures was treated by Pippard [55,1) 60,2)], using the considerations of interaction with the electron gas as a whole. In the high-frequency limit his expression goes over into Makinson's results for the attenuation of lattice waves. The reason why Pippard's theory spans both regions will be discussed in the next section.

1.2.2. *Absorption of longitudinal sound waves*

The normal metal is assumed to contain N free electrons per unit volume, occupying all velocity states up to the Fermi velocity v_F. During the passage of the sound wave the local density of the electrons fluctuates periodically, and the lattice acquires some local velocity. Thus the instantaneous equilibrium Fermi surface is of a different radius than the initial one, and has shifted slightly in momentum space. Because the electron distribution requires a finite time τ, the relaxation time, to adjust to changes in the instantaneous equilibrium, the actual Fermi surface, which also changes periodically, always lags a little behind the instantaneous equilibrium. The resulting irreversible processes lead to a net energy absorption.

In this way Pippard obtained the following expression for the absorption of longitudinal sound waves

$$\alpha_l = \frac{Nm^*}{\rho c_l \tau}\left(\frac{1}{3}\frac{(q\bar{l})^2 \arctan(q\bar{l})}{(q\bar{l}) - \arctan(q\bar{l})} - 1\right), \tag{5}$$

where ρ is the density of the metal, c_l the velocity of longitudinal sound waves, q the wave number of the sound waves, and $\bar{l} = v_F\tau$ the mean free path of the conduction electrons. Pippard's derivation holds for all values of $q\bar{l}$. In (5) it

is assumed that $\omega\tau \ll 1$, which is always the case for the ultrasonic waves used in our experiments.

The results for the low-frequency limit of (5) could also be obtained by a viscosity approximation, where the local velocity of the lattice is taken as uniform. Expression (5), however, claims validity for $q\bar{l} \gg 1$ as well. In that case it takes the form

$$\alpha_l = \frac{\pi N m^* v_F \omega}{6\,\rho c_l^2} + \text{a term independent of frequency}. \qquad (6)$$

The absorption is then independent of the relaxation time τ and varies linearly with the frequency.

For $q\bar{l} \gg 1$, a quantum-mechanical treatment of electron-phonon interaction can be used to derive an expression for the absorption of longitudinal sound waves. This expression was derived by Makinson for the absorption coefficient of lattice waves due to the interaction with conduction electrons [56,2] *), namely

$$\alpha = \frac{\hbar}{2\,\pi\rho c^2}\,\omega C^2 \left[k^2\left(\frac{\mathrm{d}k}{\mathrm{d}E}\right)^2\right]_{E_F}, \qquad (7)$$

where c is the velocity of the sound, k the wave number and E the energy of the conduction electrons. The expression in square brackets is taken at the Fermi energy E_F. The parameter C, having the dimensions of energy, is the electron-phonon interaction constant, defined by $H' = C\varepsilon\psi^*\psi$, where ψ is the wave function of the electron and ε the dilatation **). It will readily be seen that for a free-electron gas this expression agrees with equation (6) if one takes $C = \frac{2}{3} E_F$. If one estimates C by a deformation-potential argument one does indeed obtain that $C = \frac{2}{3} E_F$ [60,3] in the simplest case. Since Pippard's argument of charge neutrality involves the deformation potential when he considers the above-mentioned change in the radius of the Fermi surface, it is not surprising that this result agrees with equation (7).

In figure 4 the absorption multiplied by a frequency-independent factor is plotted against wave number times mean free path of the conduction electrons. Equation (6) shows that the value of v_F can be deduced from the slope of the asymptote to this graph.

The band-structure model of the electrons would lead to a more complicated theory for the absorption of longitudinal sound waves than the above-mentioned theories, which are all based on the concept of the free electron. If for instance the Fermi surface of the electrons runs through the first and second Brillouin zones, the energy levels in the two zones may be differently affected by uniform compression in the sound-propagation direction [55,2]. Furthermore

*) The same expression was derived independently by Morse [59,3].

**) Note, however, that some authors, e.g. Klemens [56,2], define this C by $H' = \frac{3}{2} C\epsilon\psi^*\psi$, and hence obtain an expression for α which is $^4/_9$ times the expression given in equation (7).

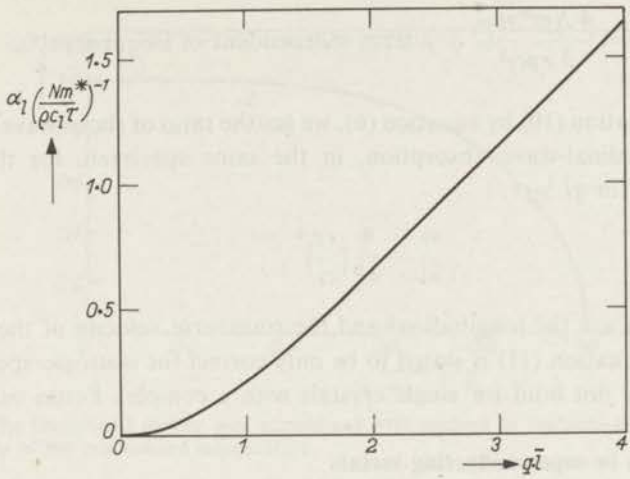

Fig. 4. Reduced absorption for longitudinal sound waves as a function of wave number times mean free path of the conduction electrons.

a periodic transfer of electrons between the zones may occur owing to the passage of a sound wave. Whether the relaxation time appropriate for this situation can be equated to the relaxation time for free electrons is still an open question.

1.2.3. *Absorption of shear sound waves*

The absorption of transverse sound waves, generally called shear waves, will now be discussed briefly. Shear waves do not cause density changes in the sound-propagation direction. But on the other hand the electronic-current density and the lattice-current density do not cancel out; there is thus a magnetic field perpendicular to the propagation direction and to the polarization direction of the sound. This induces an electric field in the polarization direction.

Pippard has taken into account this induced electromagnetic field as well as the effect of collisions on the deviation from the equilibrium Fermi velocity. He has evaluated the shear-wave absorption in a similar way as the longitudinal-wave absorption to be

$$\alpha_t = \frac{Nm^*}{\rho c_t \tau} \frac{1-g}{g}, \tag{8}$$

where

$$g = \frac{3}{2(q\bar{l})^2} \left\{ \frac{(q\bar{l})^2 + 1}{q\bar{l}} \arctan(q\bar{l}) - 1 \right\}. \tag{9}$$

A plot of α_t against $q\bar{l}$ looks much like figure 4. For $q\bar{l} \gg 1$ one gets $g \to 3\pi/4\, q\bar{l}$, and

$$a_t = \frac{4\,Nm^* v_F \omega}{3\,\pi\rho c_t^2} + \text{a term independent of frequency}. \tag{10}$$

Dividing equation (10) by equation (6), we get the ratio of shear-wave absorption to longitudinal-wave absorption, in the same specimen, for the same frequency and for $q\bar{l} \gg 1$:

$$\frac{a_t}{a_l} = \frac{8}{\pi^2}\left(\frac{c_l}{c_t}\right)^2, \tag{11}$$

where c_l and c_t are the longitudinal and the transverse velocity of the sound. respectively. Equation (11) is stated to be only correct for isotropic specimens, It will certainly not hold for single crystals with a complex Fermi surface.

1.3. Absorption in superconducting metals

1.3.1. *The physical meaning of the energy gap*

In a normal metal all electrons can be excited independently of each other, the only restriction being the Pauli principle. Excitation of a single electron from the ground state means, when wave-vector representation is used, that an electron leaves its place at $\mathbf{k} = \mathbf{k}_i$, where $|k_i| < |k_F|$ and settles at $\mathbf{k} = \mathbf{k}_j$, where $|k_j| > |k_F|$, leaving a hole at $\mathbf{k}_i$. In these inequalities $\mathbf{k}_F$ is the Fermi wave vector. The energy difference between the ground state and the excited state is given by

$$\Delta E = \varepsilon_j - \varepsilon_i = |\varepsilon_j| + |\varepsilon_i|, \tag{12}$$

where ε_i and ε_j denote the energies with the Fermi energy E_F as zero point; for simplicity the assumption is made that in **k**-space the Fermi surface lies far from a zone boundary. All single-electron excitations, even of infinitely small ΔE, are possible in normal metals.

In contrast to normal metals, there is always a lower limit to the excitation energy ΔE in superconductors; in other words, there is an energy gap between the ground state and the single-particle excited states for superconductors. The energy difference between the ground state and an excited state is represented by an equation similar to (12):

$$\Delta E = (\varepsilon_j^2 + \Delta^2)^{1/2} + (\varepsilon_i^2 + \Delta^2)^{1/2}. \tag{13}$$

The quantity 2Δ, which we shall call the energy gap, is thus *the lowest possible energy for breaking up a pair of electrons*. Strong experimental evidence for the existence of such an energy gap has been provided by measurements of the transmission and the reflection of infrared radiation [57,2]) and of the surface impedance for microwaves [59,4]) of superconducting metals.

Bardeen, Cooper and Schrieffer in their well-known paper [57,1]) gave an ex-

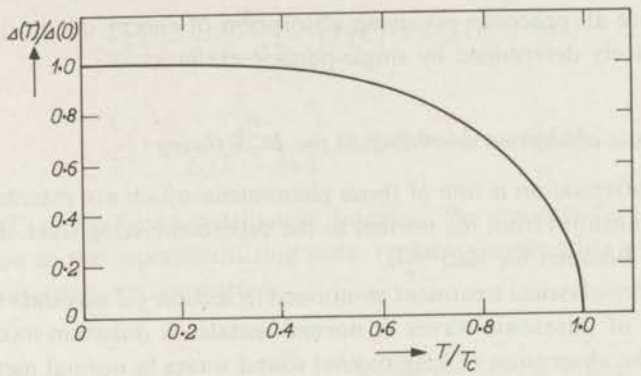

Fig. 5. The theoretical energy gap normalized with respect to the zero-temperature gap as a function of the normalized temperature.

pression for the temperature dependence of the energy gap. This energy gap increases from zero at the transition temperature T_c to about $3{\cdot}5\ kT_c$ at zero temperature, as is shown in figure 5. Although this energy gap is extremely small compared to other energies which appear in a superconducting metal, it accounts for all differences between normal and superconducting metals.

The energy gap is a consequence of the electron-electron interaction through virtual phonons, suggested by Bardeen, Cooper and Schrieffer [57,1]). This interaction has been described by Cooper [60,4]) as follows. An electron travelling through the lattice distorts the lattice, even at $T = 0$, provided that the lattice points are not infinitely heavy or rigidly fixed. Even when the electron does not have enough energy to emit a phonon with a long life time, this interaction with the lattice may let it momentarily emit a phonon existing during a very short time interval which is determined by Heisenberg's uncertainty principle. One usually says that a virtual phonon is excited by the travelling electron. The virtual phonon has a certain extension in the phonon field, and another electron may undergo its influence, which means coupling to the first electron, with conservation of the sum of their wave vectors. We shall limit ourselves to simple two-body correlations here. The interaction hamiltonian shows that this electron-electron interaction is attractive provided that the energy difference between the electron states is smaller than the virtual-phonon energy $\hbar\omega_{\mathrm{ph}}$. Opposed to this electron-electron interaction is the repulsive Coulomb interaction which is a typically short-range effect, as long-range Coulomb forces are screened by the other electrons. The criterion of Bardeen, Cooper and Schrieffer for superconductivity is that the attractive electron-electron interaction should dominate the short-range Coulomb interaction. They have shown that there is then a very strong preference for pairs of electrons having zero total wave vector and opposite spin. All other interactions typical of a normal metal are supposed not to change when the metal undergoes the transition to the superconducting

state. Therefore all processes involving absorption of energy quanta less than 2Δ are exclusively determined by single-particle excitations.

1.3.2. *Ultrasonic absorption according to the BCS theory*

Ultrasonic attenuation is one of those phenomena which are extremely sensitive to the transition from the normal to the superconducting state. This was discovered by Bömmel for lead [54,1]).

Pippard's semi-classical treatment mentioned in section 1.2 accounts fully for the behaviour of ultrasonic waves in normal metals. A quantum-mechanical treatment of the absorption of longitudinal sound waves in normal metals has been given by Makinson, see [56,2]) and by Morse [59,3]). Such a treatment is essentially limited to $q\bar{l} \gg 1$. Pippard's treatment, which is applicable to all ultrasonic frequencies and which, moreover, makes use of simple concepts, was preferred for describing ultrasonic absorption in normal metals. Ultrasonic absorption in superconductors has so far been described only by means of the concepts of quantum mechanics. The first, and still the best, description of this kind is based on the BCS theory [57,2]) [61,1]). The same perturbation hamiltonian $H' = C\varepsilon\psi^*\psi$ as for normal metals is used, but the electron wave function and the density of states are essentially different from those for the normal state.

We shall now calculate the ratio of the ultrasonic absorption in a superconductor to that in the same metal in the normal state according to the BCS theory. In order to do this we must introduce the density of states per unit of energy for one spin in the superconducting metal, $N_s(E)$. The assumption is furthermore made that the corresponding quantity for the normal state, N_n, is constant on and near the Fermi surface. It is simply shown that $N_s(E) = N_n \, \mathrm{d}\varepsilon/\mathrm{d}E$. For a superconductor equation (13) leads to $\varepsilon = (E^2 - \Delta^2)^{1/2}$, so that $\mathrm{d}\varepsilon/\mathrm{d}E = E/(E^2 - \Delta^2)^{1/2}$. Therefore [61,1])

$$N_s(E) = N_n E/(E^2 - \Delta^2)^{1/2}. \tag{14}$$

Absorption of sound with angular frequency ω involves the transition from a state of energy E to one of energy $E + \hbar\omega$. The probability of such a transition is proportional to the square of the scattering matrix element and to the density of states of the final state $N_s(E + \hbar\omega)$ [55,3]). The induced absorption is proportional to this transition probability and to the density of the initial state $N_s(E)$. The measured absorption is equal to the difference between induced absorption where the energy increases from E to $E + \hbar\omega$ and induced emission where the energy decreases from $E + \hbar\omega$ to E.

The mean square matrix elements for transitions from E to $E + \hbar\omega$ and from $E + \hbar\omega$ to E have been evaluated by Bardeen, Cooper and Schrieffer in their well-known paper [57,1]). They are, respectively,

$$\frac{1}{2}\left(1-\frac{\Delta^2}{E\,(E+\hbar\omega)}\right) f(E)\{1-f(E+\hbar\omega)\}$$

and

$$\frac{1}{2}\left(1-\frac{\Delta^2}{E\,(E+\hbar\omega)}\right) f(E+\hbar\omega)\{1-f(E)\}\,,$$

where $f(E)$ is the Fermi distribution function. We can therefore write for the absorption in the superconducting state, replacing summation over the quasi-continuous states by integration:

$$\alpha \sim 2\int_{\Delta}^{\infty}\left(1-\frac{\Delta^2}{E\,(E+\hbar\omega)}\right)[f(E)\{1-f(E+\hbar\omega)\}+$$

$$-f(E+\hbar\omega)\{1-f(E)\}]\,N_s(E)\,N_s(E+\hbar\omega)\,\mathrm{d}E=$$

$$=2\int_{\Delta}^{\infty}\left(1-\frac{\Delta^2}{E\,(E+\hbar\omega)}\right)\{f(E)-f(E+\hbar\omega)\}\,N_s(E)\,N_s(E+\hbar\omega)\,\mathrm{d}E. \qquad (15)$$

The energy-dependent $N_s(E)$ is eliminated when we use (14). By putting $\hbar\omega \ll 2\Delta$, which is permissible under the experimental conditions, we get

$$\alpha_s \sim 2\int_{\Delta}^{\infty} N_n^2\{f(E)-f(E+\hbar\omega)\}\,\mathrm{d}E=$$

$$=-2\int_{\Delta}^{\infty} N_n^2\hbar\omega\,\frac{\mathrm{d}f}{\mathrm{d}E}\,\mathrm{d}E=2\,\hbar\omega N_n^2 f(\Delta)\,. \qquad (16)$$

For the absorption in the normal metal we get the same expression, except that $\Delta=0$, and therefore the integral has to be taken from 0 to $+\infty$. This gives

$$\alpha_n \sim 2\int_{0}^{\infty} N_n^2\{f(E)-f(E+\hbar\omega)\}\,\mathrm{d}E=-2\int_{0}^{\infty} N_n^2\hbar\omega\,\frac{\mathrm{d}f}{\mathrm{d}E}\,\mathrm{d}E=$$

$$=2\,\hbar\omega N_n^2 f(0)=\hbar\omega N_n^2\,, \qquad (17)$$

whence

$$\frac{\alpha_s}{\alpha_n}=2f(\Delta)\,. \qquad (18)$$

Here $f(\Delta)$ is the Fermi distribution function at the gap boundary, which is

given by $(e^{\Delta/kT} + 1)^{-1}$, where k is the Boltzmann constant.

This ratio a_s/a_n was evaluated by using the perturbation hamiltonian H', defined above. Therefore one should expect equation (18) to be valid only for $q\bar{l} \gg 1$. Tsuneto [61,3]) has shown, however, that equation (18) should also hold for $q\bar{l} < 1$. This does not sound unreasonable, because both the electron wave function and the density of states are defined independently of the value of $q\bar{l}$.

The energy gap was assumed by Bardeen, Cooper and Schrieffer to be isotropic. This assumption is not always valid: measurements by Morse et al. [59,5]), and by Bezuglyĭ et al. [61,2]) on superconducting tin have given evidence for gap anisotropy in this metal, see figure 6. But in this theoretical section the gap will be assumed to be isotropic.

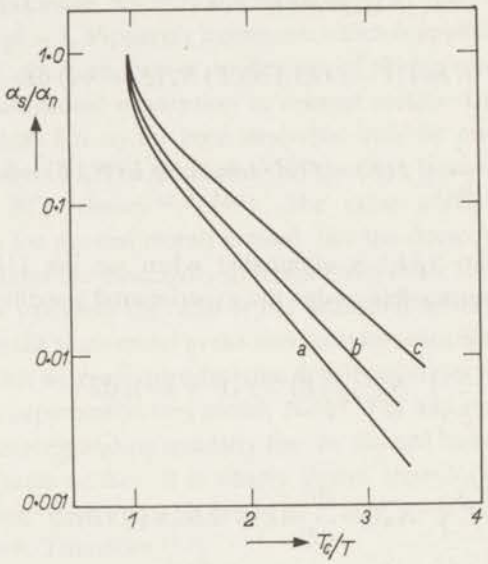

Fig. 6. The absorption normalized with respect to the normal-state absorption as a function of T_c/T, after Morse et al., for three different propagation directions in a tin single crystal. From the slope of (*a*), (*b*) and (*c*) the zero-temperature energy gap may be calculated for the three propagation directions.

Finally figure 7 shows some experimental results for longitudinal sound waves in tin and indium, obtained by Morse and Bohm [57,3]), compared to the theoretical curve predicted by BCS. It will be seen that the agreement is reasonable, although the relatively small deviations for $T > 0{\cdot}7\ T_c$ still have to be explained.

1.3.3. *Absorption of shear waves in superconducting metals*

At frequencies where $q\bar{l} > 1$ the shear-wave attenuation decreases much faster just below the superconducting transition temperature T_c than the BCS theory

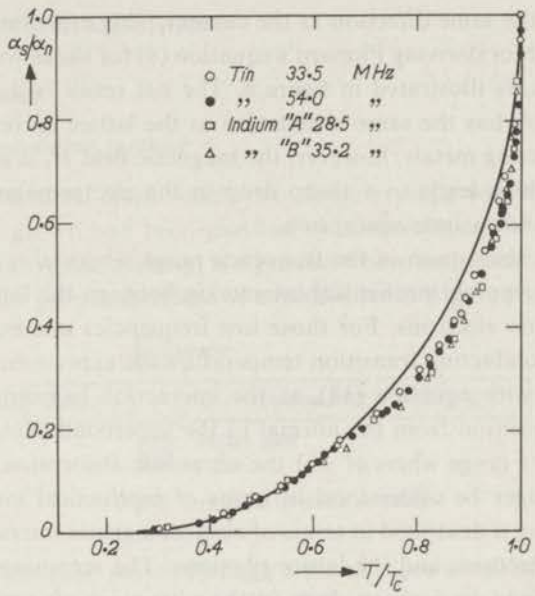

Fig. 7. Normalized absorption as a function of normalized temperature for longitudinal sound waves in tin and indium, after Morse and Bohm. The full curve is the theoretical curve according to BCS.

predicts [59,2] [62,1] [63,4]). This sudden change in the shear-wave attenuation can be understood qualitatively in the following way.

In a normal metal the elastic deformation of the lattice by the sound waves implies an oscillating lattice current of the same frequency as that of the sound waves. The propagation of this electric current has the same direction as the polarization of the sound waves, i.e. perpendicular to the propagation direction of the sound waves. The electric current causes an alternating magnetic field H_t perpendicular to the polarization direction, and this in turn an electric field E_t,

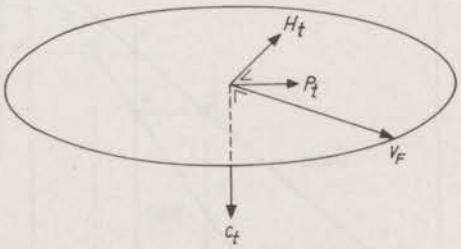

Fig. 8. Diagram for shear-wave absorption at low temperatures;
c_t = propagation direction of sound wave,
P_t = electric polarization of lattice,
H_t = magnetic field due to sound wave,
v_F = velocity component of an electron contributing to the absorption.

which again has the same direction as the current. This mechanism, which has already been used for deriving Pippard's equation (8) for shear-wave absorption in normal metals, is illustrated in figure 8. The net result is a self-consistent electric field which has the same orientation as the lattice current.

In superconducting metals, however, the magnetic field H_t is screened by the supercurrents, which leads to a sharp drop in the electromagnetic induction which causes the ultrasonic absorption.

The ultrasonic absorption in the frequency range where $q\bar{l} \ll 1$ can be likewise attributed to a purely mechanical interaction between the lattice vibrations and the conduction electrons. For those low frequencies one may expect that below the superconducting transition temperature the experimental results will show agreement with equation (18), as the interaction hamiltonian does not change at the transition from the normal to the superconducting state.

In the frequency range where $q\bar{l} \gg 1$ the ultrasonic absorption in the normal metal can no longer be understood in terms of mechanical interaction. The absorption process is described in terms of electromagnetic interaction between the conduction electrons and the lattice phonons. The screening by the supercurrents should lead to a sharp drop in the ultrasonic absorption at T_c. In practice, however, the ultrasonic absorption does not decrease discontinuously, but in a range of about 0·02 T_c below the transition temperature. This may be ascribed to the fact that just below T_c there are not enough "superconducting electrons" for screening the whole induced magnetic field. Below 0·98 T_c the screening should be complete. The remaining ultrasonic absorption can be ascribed again to mechanical coupling between the lattice vibrations and the conduction electrons.

A small drop in the attenuation of longitudinal sound waves has been observed for tin and indium, leading to a poor agreement between the experiments and the BCS theory. This is shown in figure 7. The discrepancy can be understood as follows. The "longitudinal" sound waves could have small shear components. Owing to the screening process described above those components will decrease much more below the transition temperature than the compressional component.

2. EXPERIMENTAL METHOD

2.1. The specimens

2.1.1. *The zone-refining method*

The very pure metal from which two single crystals with orientation (100) and (110) were grown had been purified by zone refining [58,3]). Zone refining, and more generally zone melting, is a process where redistribution of impurities takes place at the growth interface of a molten zone. Figure 9 shows schematic-

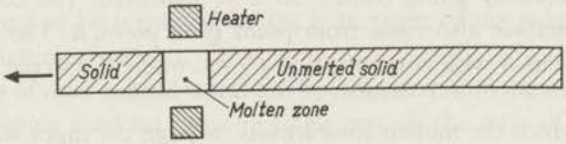

Fig. 9. Principle of zone melting.

ally how a molten zone moves through a metal ingot containing one or more solute impurities. In order to describe the zone-melting procedure we must introduce the distribution coefficient k, which is the ratio of the concentration of solute impurities at the growth interface to that in the main body of the liquid. If the concentration at the growth interface is lower than in the liquid the distribution coefficient is less than unity. The melting point of the solvent during the zone-melting procedure is then lower than if the ingot were completely homogeneous.

The procedure of zone refining can be most simply explained with reference to the phase diagram of figure 10 which refers to a single solute which has a

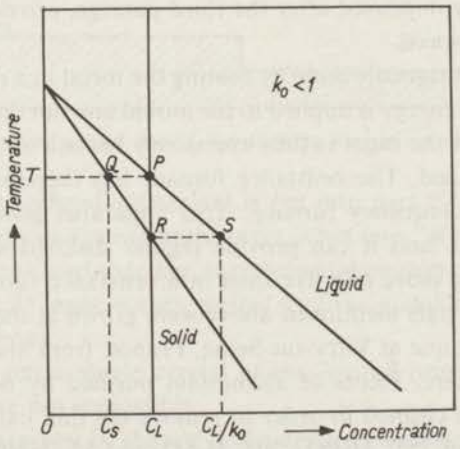

Fig. 10. Phase diagram for a binary system in which the freezing point is lowered by the solute; $C_S = k_0 C_L$.

concentration C_L in the liquid solvent. If the solution is very slowly cooled, the first solid will appear at a temperature T, say. At all points between P and Q, an equilibrium exists between liquid and solid phase. The composition of the first solid to appear at the temperature T is represented by point Q. It will contain a concentration C_S of solute in solid solution. The initial distribution coefficient k_0 is thus C_S/C_L. In general k_0 will depend on the concentration, except for very dilute solutions.

Since the solid phase is poor in the solute, the concentration in the liquid continually rises. The increment of impurity concentration in the body of the liquid is represented by going from P to S in figure 10. The concentration at the growth interface also rises, from point Q to point R. The last droplet of liquid solidifies at S with concentration C_L/k_0, where C_L is the initial concentration.

The speed at which the molten zone travels through the ingot would be unimportant, were diffusion within the liquid infinitely rapid, so that the concentration throughout the liquid zone were constant. Tiller et al. [53,1]) have shown that this assumption is not true in general, as the diffusion is normally so slow as to cause inhomogeneities in the liquid. In other words, if the molten zone moves too quickly through the liquid, the impurities will not be removed as well as is possible, while if the molten zone moves too slowly the impurities may diffuse back into the hot growth interface. The optimum melting velocity must thus be determined experimentally for each metal [55,4]). It can further be shown, that the ratio of the length of the molten zone to the total length of the ingot must be kept as small as possible.

The concentration of the solute is further diminished by repeating the zone-refining procedure after having removed the last part of the ingot, which contains most of the impurities. Montariol [55,4]) has shown that for aluminium the purification is hardly improved after the third passage, provided that the zone travels at optimum speed.

Zone refining was originally done by heating the metal in a resistance furnace. In such a furnace the energy is applied to the mould and not directly to the metal ingot. The outside of the ingot is thus excessively heated, and the molten zone is far from disk-shaped. The resistance furnace has therefore generally been replaced by a high-frequency furnace. This apparatus generates the energy directly in the metal, and it can provide regular disk-shaped molten zones, making zone melting more effective than in a resistance furnace.

The two single crystals mentioned above were grown at the Centre d'Etudes de Chimie Métallurgique at Vitry-sur-Seine, France, from aluminium that had been zone-refined there. Pieces of aluminium purified by double electrolysis were first thoroughly cleaned in order to remove the thin oxide film. This was done with a mixture of 75 % H_3PO_4, 20 % H_2SO_4 and 5 % HNO_3, and then with boiling distilled water. After that the pieces of aluminium were placed in a

carefully degassed graphite mould which was put into a quartz tube. The graphite mould is preferable to one of aluminium oxide, being less susceptible to thermal fracture. The system was evacuated, and sometimes argon was added. The various pieces of aluminium were then fused together in a high-frequency furnace with a maximum power of 6 kW at a frequency of 600 kHz. As the molten zone should be as short as possible, the nine windings of the heating coil lay partly over one another, thin sheets of teflon being used as insulation.

Zone melting was repeated several times, the metal being moved mechanically through the coil at a speed of about 3·5 cm per hour. The anode current of about 1 A had to be regulated, as the inductance of the heating coil changed during the melting process.

The purity of zone-refined metal can be estimated from the residual resistance. In the aluminium used for growing single crystals the ratio of the resistance at liquid-hydrogen temperature to that at room temperature was (5 to 6) . 10^{-4}, corresponding to about 8 p.p.m. impurities [55,5]).

2.1.2. *Growing single crystals*

Figure 11 shows the dimensions of the mould used for growing single crystals. It is made from Norton cement with a trace of aluminium oxide added to prevent silicon from contaminating the aluminium. It is baked 24 hours at 1200 °C.

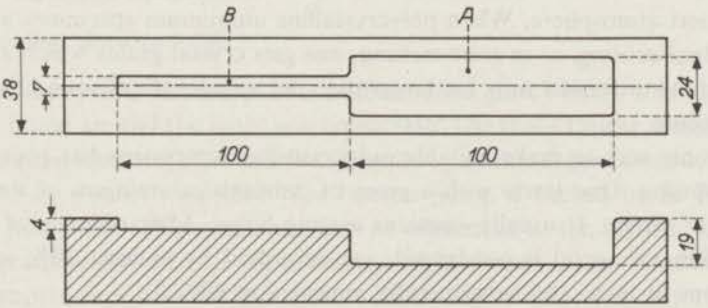

Fig. 11. Norton-cement mould for growing aluminium single crystals.

An ingot of zone-refined aluminium is put into part "*A*" of the mould. An oriented seed of the same purity as the ingot is put into "*B*", partly covering the ingot. They are then fused together, care being taken that only part of the seed is melted. The whole ingot is then melted and the metal solidified at a rate of about 1·8 cm per hour.

In general one gets a single crystal of the desired orientation in this way; twins, however, are not impossible.

The specimens can best be shaped to the desired diameter with an electrolytic saw, as this does not disturb the crystal structure even superficially. This saw

is formed by a 0·05 mm silver wire through which an electric current flows and which is surrounded by a 20% $NaNO_3$ solution, containing a small quantity of HCl to prevent hydrolysis. Only when the specimens have a diameter exceeding about 2 cm careful hand sawing is necessary. The method of cutting by electrical sparking was not yet sufficiently well known to be used when the specimens mentioned above were prepared.

2.1.3. *The crystal structure*

The orientation of the specimen axis is most easily determined by the back-reflection Laue method. This method does not require specimens of low absorption and of small thickness, like the transmission method. The orientation of the specimen axis with respect to the main crystallographic axes was read off from a Greninger chart. For both single crystals the misorientation proved to be 3°.

For the purpose of measurements with shear waves, the position of the crystallographic axes in the end faces had to be determined too. This was done by means of large-angle reflection of "white" X-rays *). The spots on the film were analyzed by means of a Wulf net. Both methods have been described at length by Cullity [56,3].

2.1.4. *Making polycrystalline specimens*

Cast aluminium always contains casting holes, even when cooled slowly and in an inert atmosphere. When polycrystalline aluminium specimens are made by gradual cooling, as in zone melting, one gets crystal grains which are sometimes of the order of 1 mm, i.e. larger than the wavelength of sound used in the experiments.

The only way to make suitable polycrystalline specimens has proved to be the following. One starts with a piece of industrial aluminium of the desired degree of purity. It usually contains casting holes. After removal of the thin oxide film the metal is hot-forged, i.e. deformed by at least 30% in several directions in turn, and subsequently annealed at 600 °C.

The polycrystalline specimen mentioned in chapter 3 was made in this way.

2.1.5. *The coupling seal*

A thin coupling film is necessary for transferring the mechanical vibrations from the quartz transducer to the specimen. This film must be rather viscous for transferring shear waves at room temperature. The ideal coupling liquid would have an acoustic impedance which is the geometric mean of the acoustic

*) I wish to thank Ir J. A. Kloosterman, Instituut voor Metaalkunde van de Technische Hogeschool, Delft, for his help in analyzing crystal orientations and for preparing a polycrystalline specimen.

impedances of the quartz crystal and of the specimen. This is, however, by no means necessary.

Several investigators have made use of the Dow Corning silicone oil with a viscosity of 2,500,000 centistokes at 25 °C. A more handy fluid is "Nonaq" stopcock grease, made by Fisher Scientific Comp., Fair Lawn (N.J.). It dissolves in water and in alcohol, but not in other organic liquids. Because of its solubility in water, a new coupling film must be made for each low-temperature experimental run, unless the specimen is kept in vacuum or in a dry atmosphere, for instance in helium gas.

Nonaq is fairly fluid at room temperature, but it becomes stiff at about 150 °K. Sometimes this transition causes cracking of the seal which makes measurements below that temperature impossible. Very rapid cooling of the specimen from room temperature to liquid-nitrogen temperature proves to be the best way to avoid this effect [63,3]). The seal is then kept intact and no damage occurs to it when the specimen is cooled down further to liquid-helium temperatures. A possible explanation for this is that Nonaq has a very large specific heat compared to that of the metal specimen and of the transducer.

Because of the phase transition of the coupling seal, measurements at room temperature cannot be combined directly with measurements at low temperatures.

2.2. The cryogenic equipment

2.2.1. *Cooling down to* 1 °K

The Dewar system consists of two double-walled glass vessels. The outer one contains liquid air and the inner one liquid ^{4}He. The inner Dewar vessel, which has an internal diameter of 54 mm is connected to a three-stage Edwards booster pump 9B3 by a short wide tube. The booster pump is backed by an Edwards rotation pump 1SC450B which can also be connected to the cryostat directly.

Temperatures down to 1·3 °K are obtained by means of the rotation pump only. Temperatures between 1·3 and 0·9 °K can be obtained by adjusting the pumping speed of the booster pump. As the superconducting transition temperature of the aluminium specimens is 1·16 to 1·17 °K, part of the superconducting region can be covered with the aid of the booster pump. The temperature can then be determined by reading the pressure over the ^{4}He bath by means of a MacLeod manometer. This method is not suitable for keeping the temperature constant. It is therefore preferable to cool the ^{4}He bath down to 1·3 °K and to adjust the temperature by controlling the ^{3}He pressure. For temperatures below 0·9 °K the ^{4}He bath is set at 0·9 °K with the booster pump.

2.2.2. *The* ^{3}He *cryostat*

The two normal methods for cooling specimens to well below 1 °K are the

adiabatic-demagnetization method and the ^{3}He-evaporation method.

When one uses adiabatic demagnetization one converts the superconducting aluminium into normal metal by applying a large magnetic field. Very pure aluminium may take a very long time to become fully superconducting without normally conducting regions after the magnetic field is switched off. This cooling method is therefore highly unsuitable for use in investigations of the properties of superconducting aluminium of a very high degree of purity.

A ^{3}He cryostat is a convenient means of cooling the specimen to temperatures between 0·4 and 0·5 °K, and keeping the temperature constant for one measurement. A number of ^{3}He cryostats have been developed in various countries [61,4]). In some of them the ^{3}He is recirculated because of a relatively large heat input. Our ^{3}He cryostat is fairly simple, as no recirculation is needed. About 0·5 cm^3 of liquid ^{3}He is sufficient for several runs taking at least two hours in all.

The pumping set-up is sketched in figure 12. The pumping speed of the Balzers pump "Duo 1", carefully made free of leaks to prevent loss of ^{3}He, is adjusted by means of the two valves 8 and 9, connected in parallel. One end of the oil manometer 4 is connected to the ^{3}He bath, and the other end to the high-vacuum mercury diffusion pump, which also provides a pressure of the order of 10^{-6} mm Hg in the space surrounding the liquid ^{3}He.

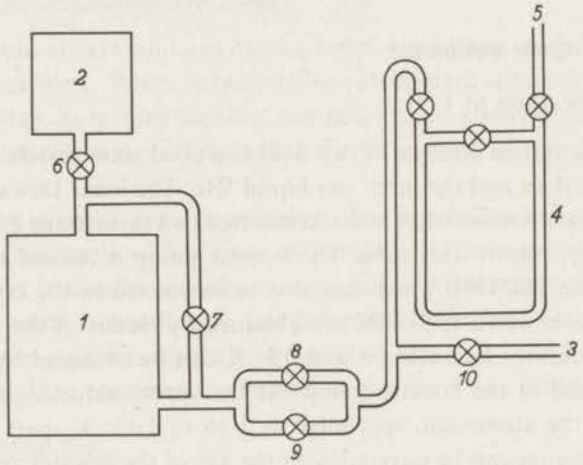

Fig. 12. ^{3}He line.
1 = Balzers pump.
2 = ^{3}He container.
3 = to cryostat.
4 = oil manometer.
5 = to mercury diffusion pump.
6 = container valve.
7 = short-circuit valve.
8 = control valve.
9 = shunt valve.
10 = cryostat valve.

The cold part of the equipment is shown in figure 13. The ^{3}He vessel *f*, which is surrounded by ^{4}He gas, has an internal diameter approximately 2 mm larger than that of the specimen *a*; this gives good thermal contact between the specimen

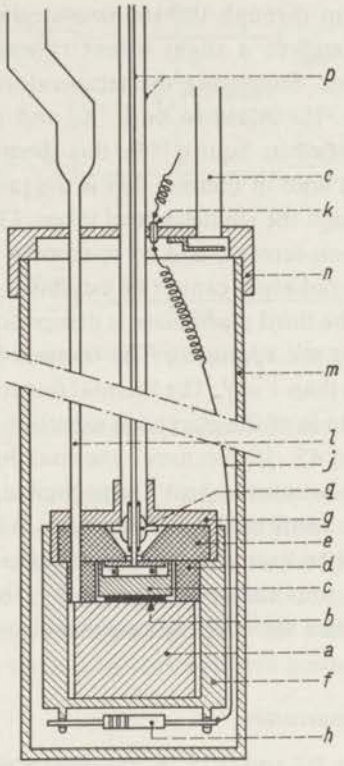

Fig. 13. Cold part of the ^{3}He cryostat.
a = specimen.
b = transducer.
c = spring-mounted electrode.
d = lorrival spacer.
e = lorrival ring.
f = specimen container.
g = cover.
h = thermistor.
j = thermistor filament.
k = bead.
l = ^{3}He condenser tube.
m = vacuum vessel.
n = cover.
o = pumping tube.
p = coaxial lead.
q = bead.

and the liquid ^{3}He. The condenser tube *l* with a simple radiation shield may be seen on the left, and on the right the tube *o* leading to the high-vacuum mercury diffusion pump, with a radiation screen below it. The coaxial lead *p* is carefully soldered to the cover *g* with silver solder. When the specimen has been mounted, the specimen container *f* and the high-vacuum vessel *m* are attached to their cover by Wood's metal. All other soldering is done with tin solder. The tubes leading to the ^{3}He vessel are made of stainless steel.

For practical reasons it is not possible to bring the thermistor into close contact with the specimen. Mounting the thermistor on the bottom of the ^{3}He box does not cause a measurable error in determining the temperature, provided the heat dissipation in the thermistor amounts to less than 2.10^{-10} W.

The thermal flux to the ^{3}He bath and the specimen comes from three sources.

First there is conduction through the stainless-steel condenser tube *l* and the electrical connections, and to a slight extent through the constantan wires leading to the thermistor. Supposing the temperature of the ^{4}He bath to be 1·0 °K and that of the ^{3}He liquid to be 0 °K, and making use of the heat-conductivity data published by Squire [53,2]), this thermal flux can be estimated to be 3 μW. The second kind of thermal flux is the radiative, both through the vacuum space and through the stainless-steel tubes. This last contribution has been reduced by radiation screens, and by spacers in the coaxial connections. The thermal flux due to radiation cannot be estimated, but there is no evidence that it is important. In the third place there is dissipation of electric energy both in the thermistor and in the specimen. The thermal flux to the thermistor is always considerably less than 1 μW. The thermal flux to the specimen is strongly dependent on the amplitude of the electronic signal. A large signal of say 100 V p.t.p. and a duty cycle of $45 \cdot 10^{-6}$ causes a thermal flux of the order of 3 mW. It follows that all other sources of heat are negligible compared to the pulsed oscillator. This has been confirmed experimentally. When it is necessary to use a large electronic signal to excite the quartz transducer, the signal from the pulsed oscillator is fed into the cryostat only for short periods in order to prevent the specimen from warming up appreciably, or the repetition rate is reduced.

2.2.3. *Measuring the temperature*

Temperatures between 1·2 and 0·55 °K are most easily measured by reading the vapour pressure of the ^{3}He on an oil manometer filled with "Octoil S". In order to be sure that the pressure read on the manometer really corresponds to the temperature of the liquid ^{3}He, one must shut the valves connecting the cryostat to the Balzers pump before measuring the temperature. When the electronic signal to the quartz transducer is not too large, the pressure can be kept constant for at least one minute.

Data published by Roberts and Sydoriak [56,4]) indicate that no correction need be made for the thermomolecular-pressure effect down to 0·5 °K. But below 0·55 °K the oil manometer is not sensitive enough to determine temperatures with sufficient precision. Therefore the lowest temperatures are measured by means of a Speer carbon resistor of 470 Ω at room temperature. It is part of a simple Wheatstone bridge, which is shown in figure 14. Zero voltage is indicated on a highly sensitive Philips millivoltmeter GM 6020 having an internal resistance of 1 MΩ.

According to Nicol and Soller [57,4]) the resistance of the thermistor obeys the relationship

$$T = A \log R/(\log R - B)^2 \qquad (19)$$

down to 0·3 °K, A and B being constants that can be obtained by calibration.

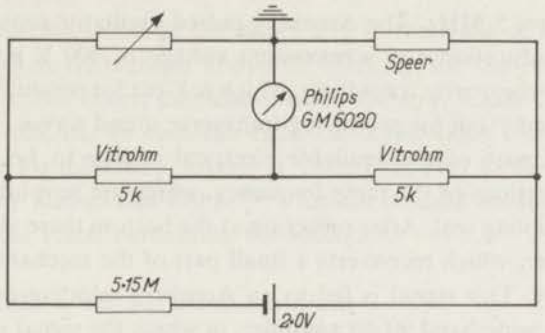

Fig. 14. Wheatstone bridge for measuring thermistor resistance.

The thermistor used was calibrated at temperatures above 0·55 °K during each series of measurements.

The 1957 ^{3}He temperature scale [57,5]) has been used throughout this thesis. The T_{62} ^{3}He scale which was recently proposed yields values of the temperature which are slightly lower than those according to the 1957 ^{3}He scale. According to the T_{62} ^{3}He scale, the superconducting transition temperature of aluminium is 6 millidegrees lower than that on the 1957 ^{3}He scale. At 1 °K the difference is 7 millidegrees and at the lowest temperatures occurring during the measurements 8 millidegrees.

2.3. The electronic equipment

2.3.1. *The block diagram*

Figure 15 shows the block diagram of the electronic equipment used at

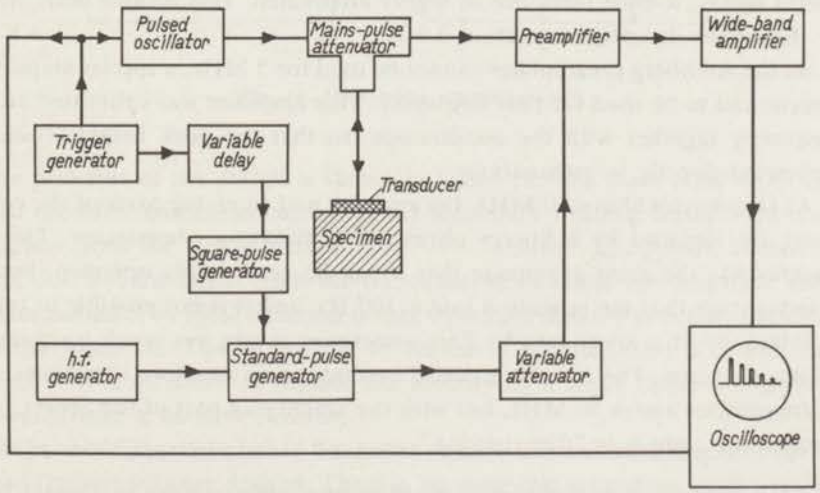

Fig. 15. Block diagram of the electronic equipment.

frequencies above 5 MHz. The Arenberg pulsed oscillator provides h.f. pulses of about $1\frac{1}{2}$ μs duration and a maximum voltage of 300 V p.t.p. over 93 Ω. These are fed to the quartz transducer, which is *X*-cut for producing longitudinal sound waves, and *Y*-cut for producing transverse sound waves. This transducer causes a small part of the available electrical energy to be converted into mechanical vibrations of the same frequency, which are sent into the specimen through the coupling seal. After reflection at the bottom these vibrations return to the transducer, which reconverts a small part of the mechanical energy into electrical energy. This signal is fed to an Arenberg selective preamplifier and from there to a wide-band 90 db amplifier, in which the signal is also detected, and ultimately to a Tektronix oscilloscope 541, where the successive reflections are displayed as peaks of decreasing amplitude.

The oscilloscope is triggered by the same pulse as the pulsed oscillator, provided by a Hewlett & Packard square-pulse generator 212A. The repetition rate is 30 per second.

As the amplifying system cannot be supposed to be linear, except for the first tube of the first amplifier, one has to make use of a standard signal of the same frequency as that emitted by the pulsed oscillator. This standard signal is modulated by a 40 V negative square pulse which comes from the square-pulse generator with some delay with respect to the trigger pulse. It is fed to the second stage of the preamplifier and also displayed upon the screen of the oscilloscope. Its height is adjusted to that of one of the reflection peaks by means of a Rohde & Schwarz unbalanced standard attenuator.

A single-transducer acoustical system would cause the main pulse to be fed to the preamplifier together with the much smaller signal from the specimen. The former would swamp the first stage of the amplifier, thus drowning the useful signal; it must therefore be highly attenuated. This is done with the aid of the circuit described in section 2.3.2.

As the Arenberg preamplifier cannot be used for 5 MHz, a special amplifying system had to be used for that frequency. This amplifier was calibrated at that frequency together with the oscilloscope, so that the peak heights could be converted directly to attenuations.

At frequencies above 50 MHz, the emitting and receiving parts of the equipment are replaced by a Sperry ultrasonic attenuation comparator. This apparatus has the great advantage that it can be very simply operated, but the disadvantage that the repetition rate is 100 Hz, and it is not possible to trigger it externally at a lower rate *). This sometimes causes too much warming up of the specimen. The Arenberg pulsed oscillator was therefore sometimes used at frequencies above 50 MHz, but with the amplifying part of the Sperry pulse comparator, which is "free-running".

*) The newer type of the Sperry ultrasonic attenuation comparator can be triggered at any rate between 10 Hz and 2 kHz.

Alternating-current losses in the cables and in the walls of the cryostat are strongly reduced at frequencies above 50 MHz by the use of line stretchers combined with a stub tuner, manufactured by General Radio Corporation. At each frequency one has to tune the electrical connections from the specimen to the amplifier for minimum losses. A tuning set next to the specimen, like that proposed by Kamm and Bohm [62,3]) cannot be used because of the small dimensions of the vessel containing the specimen.

2.3.2. *Some details of the electronic equipment*

The main-pulse attenuator

This device passes the signal from the specimen with little loss, but attenuates the main signal by about 60 db. It consists of a small ring of ferroxcube IVb, through which are threaded three wires; two of them pass straight through, while the third is wound three times round the ring, one end of this wire being earthed via the brass housing of the ferroxcube ring.

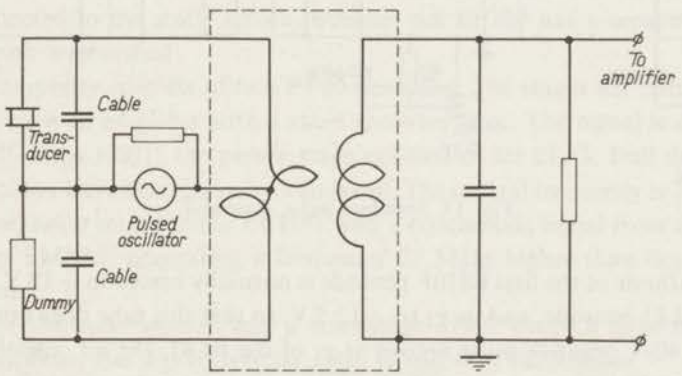

Fig. 16. Main-pulse attenuator.

The principle of the design is shown in figure 16. The main pulse from the pulsed oscillator causes no current in the secondary winding because the contributions from the two primary "turns" — "wound" in opposite senses — cancel out, but the signal from the transducer does reach the amplifier after transformation. The ideal situation is that where the dummy is exactly identical with the specimen. This is difficult to realize in practice, and is in fact not necessary. It is sufficient to replace the dummy by a small variable capacitor in parallel with a variable resistor.

The kind of ferroxcube has to be chosen so as to minimize the magnetic losses for the frequency range desired. There is no magnetic saturation, owing to the relatively small signals from the specimen.

The standard-pulse generator

The simplest way to synchronize a standard-pulse generator with a given pulse train is to have a gate connection, where a tube is normally cut off but conducts or even amplifies a signal when a square pulse fed to one of its grids opens the tube. A variation of this principle is shown in figure 17 *).

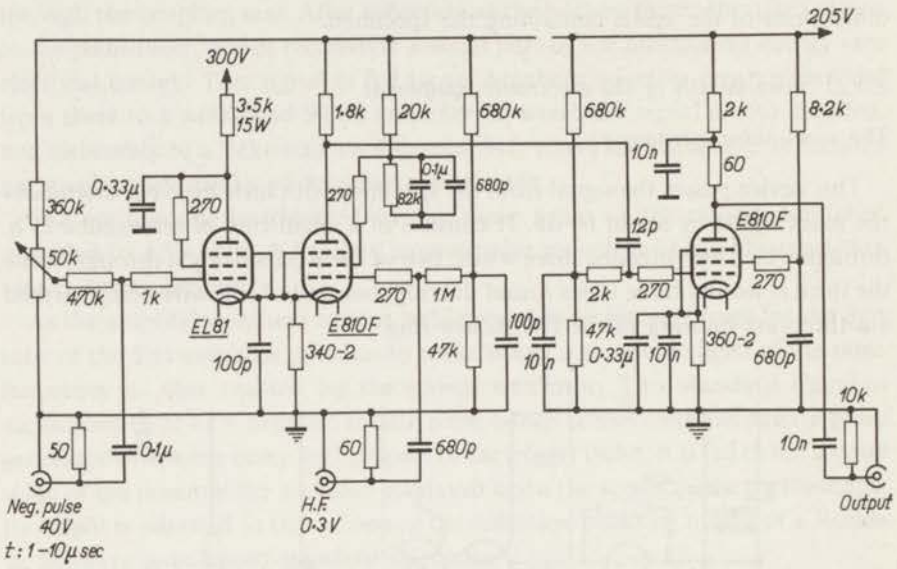

Fig. 17. Standard-pulse generator.

The cathode of the first E810F pentode is normally biased to +18 V, provided by the EL81 pentode, and its g_1 to +12·5 V, so that this tube does not conduct. When a 40-V negative pulse arrives at g_1 of the EL81, the h.f. signal fed to g_1 of the first E810F can be amplified, while a negative pulse of nearly —80 V is also produced at the anode. A differentiating network causes the second E810F to be shut for a time which is very short compared to the pulse length. After that very short time the h.f. pulse is amplified in the normal way.

The high-frequency anode resistance of the second E810F is chosen as 60 Ω, thus providing good matching with the Rohde & Schwarz attenuator which has an input resistance of 60 Ω.

The amplifier used for 5 MHz

The greater part of the amplifier is identical with that described by Van Iersel [59,6]) in his thesis. The preamplifier had originally been designed for a central frequency of 7 MHz and a bandwidth of 8 MHz. This part of the ampli-

*) I wish to thank Mr. R. Hulstman for his help in constructing this apparatus.

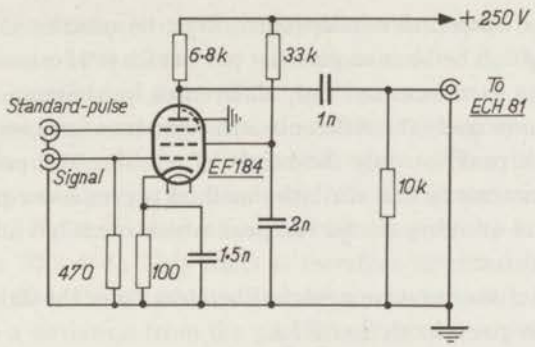

Fig. 18. First stage of amplifier for 5 MHz.

fier was replaced by a single stage that could be used for a wide range of frequencies. This stage is shown in figure 18. The signal from the specimen is fed to g_1 of the EF184 pentode, and the standard pulse can be fed to g_3. The anode voltage is applied to g_1 of the mixing tube ECH81.

The EF184 was preferred to the more conventional E180F, as the latter has its g_3 connected to the static screen, whereas the EF184 has a separate static screen, which we earthed.

The i.f. amplifier consists of two EF80 pentodes. The stages are inductance-coupled to give an amplifier with a short recovery time. The signal is detected by one half of an EB91; the power stage consists of an EL83. Full details of the i.f. amplifier have been given by Van Iersel. The central frequency is 27 MHz. The input signal is mixed in the ECH81 with a continuous signal from a Rohde & Schwarz SMLM, generating a frequency 27 MHz higher than that of the input signal.

Although this new version has a somewhat lower over-all gain than the original amplifier, the signal-to-noise ratio is still very favourable.

2.4. Ultrasonic attenuation measurements in solids

2.4.1. *General remarks*

The attenuation is determined from the signal displayed upon the screen of an oscilloscope, which is a series of peaks of decreasing amplitude, the distance between two successive peaks corresponding to twice the length of the specimen. The simplest case is that where the decay of the peaks is exactly exponential. One can then read the attenuation directly by adjusting a calibrated exponential curve to the peaks. When one wants to avoid using this calibrated curve, or when the peaks do not decay exponentially, one can either read the difference between the heights of the first or second peak and of a later peak, or only read the height of one of the later peaks.

It will be shown in section 2.4.2 that a number of contributions to the atten-

uation which are temperature-independent must be subtracted from the total measured attenuation before one gets that part which is of interest to our work. Since one thus in fact measures only differences in attenuation, it does not matter whether one reads the difference in height between two peaks, say the 2nd and the 10th peak, or only the height of e.g. the 10th peak. Morse [59,3]) has shown experimentally that the latter method is even more precise than the former. In general one chooses the last peak which is easily visible throughout one experimental run.

The principle of the measurement will be clear from the description of the measuring circuit given in section 2.3.1.

In some series the attenuation is so large that only one peak is visible upon the screen. Measurements are then made on this peak. The visibility of this peak at optimum signal-to-noise ratio of the amplifying system determines the highest relative attenuation which is measurable.

2.4.2. *Corrections*

Several corrections have to be made in order to find the attenuations in which we are interested.

The first correction is the apparent extra attenuation due to *diffraction of the sound beam*. Seki et al. [56,5]) have calculated this effect, which only gives a small contribution. They assume that the transducer vibrates uniformly and harmonically as a circular piston, and that the lateral boundaries of the specimen are far enough from the sound beam to have a negligible effect. We are only interested in those cases where the wavelength of the sound λ is considerably shorter than the radius of the source a. For these cases Seki et al. have calculated the average intensity of the sound waves as a function of the distance. For $a^2/\lambda > 2$, which holds for all measurements described in this thesis, this attenuation due to diffraction is to a good approximation proportional to the distance, and amounts to about λ/a^2 db/cm. In many cases it is much smaller than the attenuation we are interested in. For 25-MHz longitudinal sound waves in aluminium, a^2/λ has been calculated to be 10 cm, so that the diffraction attenuation is 0·1 db/cm.

Each *reflection* of the sound beam at the end faces causes another correction to the measured attenuation [63,1]). The ratio of the amplitude of the reflected sound beam to that of the perpendicularly incident sound beam is given by

$$R' = \frac{\rho_1 c_1 - \rho_2 c_2}{\rho_1 c_1 + \rho_2 c_2}, \tag{20}$$

where ρ_1 and c_1 are the density and the sound velocity for the specimen and ρ_2 and c_2 the same quantities for the adjacent medium. For an aluminium specimen, one end face of which is covered by a layer of "Nonaq", and the other by liquid ^{3}He, equation (20) gives $R' > 99\%$ at the ^{3}He end and

$R' \approx 85\%$ at the transducer end. It is possible to determine by experiment the exact contribution of this effect, but we did not need to do this.

Insufficiently parallel end faces of the specimen cause an apparent increase in the attenuation, and moreover deviations from the exponential decay of the successive peaks on the screen of the oscilloscope. When the angle between the sound beam radiated perpendicularly from the transducer and the sound beam which hits the transducer after reflection is given by $\theta = \lambda/4a$, the loss in amplitude is 30% [62,4]). This effect is therefore largest for the highest frequencies. For 100-MHz longitudinal sound waves in aluminium this angle θ corresponds to a deviation from the parallel of about 3 μ. As the ends of the specimens were hand-lapped carefully flat and parallel to within 1 μ this effect is certainly much less than the above-mentioned 30%, and can probably be neglected.

The effect of a seal layer of non-uniform thickness, due to *flexing of the transducer*, is more complicated [56,6]).

All the additional attenuations mentioned above are known to be temperature-independent below 4·2 °K. Since one may assume that the attenuation due to the electrons in the superconducting metal tends to zero when the temperature is lowered far enough below the superconducting transition temperature, the correction for the temperature-independent attenuation can be determined from the attenuation-temperature curve, as described in section 3.1.1. This dispenses with the need of calculating this correction theoretically, which is particularly useful for shear waves, on which little theoretical work has yet been done.

3. ATTENUATION AS A FUNCTION OF TEMPERATURE IN THE SUPERCONDUCTING STATE

3.1. Attenuation of longitudinal sound waves

3.1.1. *Interpretation of the measurements*

The interpretation of the experimental results described in this section is based on equation (18), derived in section 1.3.2:

$$\frac{\alpha_s}{\alpha_n} = \frac{2}{e^{\Delta/kT} + 1}, \tag{18}$$

where α_s is the absorption in the superconducting state, α_n the absorption in the normal state, and 2Δ the energy gap as defined in section 1.3.1. With this equation the value of the energy gap at $T = 0$ can be estimated following the method proposed by Morse et al. [59,5]). First one has to eliminate that part of the attenuation which is non-electronic in nature, to obtain the absorption due to the electrons. As we have seen in section 2.4.2, the non-electronic contribution α_e does not depend on the temperature in the range we are interested in. We cannot calculate this contribution accurately enough for our purposes, but we can estimate it from the experimental data on the assumption implicit in equation (18) that the electronic absorption tends to zero at $T = 0$. This can be done either by finding the value of the additive constant which gives the best fit between the theoretical BCS curve of absorption against temperature and the experimental points, particularly at low temperatures, or by plotting $\log \alpha_s$ against T_c/T for different values of α_e until the curve becomes most nearly asymptotic. The former method has been preferred as being less elaborate and apparently resulting in the same accuracy as the latter.

Using the values of the electronic absorption α_s, estimated in this way, we now calculated the ratio α_s/α_n; $\log(\alpha_s/\alpha_n)$ was plotted against T_c/T, and the energy gap at zero temperature was determined from the slope of the asymptote to the curves at the lowest temperatures. This is shown in figure 19, for the absorption of 36-MHz sound in the (100) single crystal.

The inaccuracy in determining the zero-temperature energy gap is $0{\cdot}2\ kT_c$, for each separate experimental run.

3.1.2. *The single crystals of zone-refined aluminium*

In two zone-refined aluminium single crystals of axis orientation (100) and (110), respectively, attenuation of longitudinal sound waves along the main axis was measured at different frequencies. An X-cut quartz crystal with main resonance frequency of 5 MHz was used for producing and for detecting the sound waves at all frequencies. The results for the (100) single crystal, corrected for zero attenuation and normalized with respect to α_n, are plotted against the

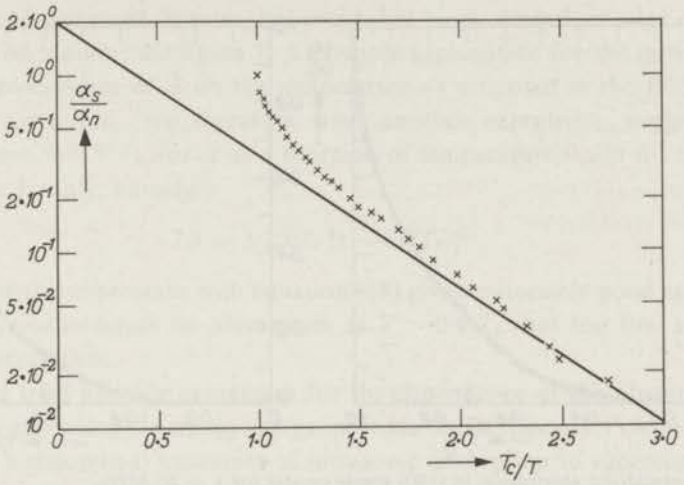

Fig. 19. (α_s/α_n) plotted on a logarithmic scale as a function of T_c/T for (100) single crystal at 36 MHz. The slope of the asymptote to this curve leads to an energy gap of 3·5 kT_c at $T = 0$.

normalized temperature in figures 20 to 23, for the frequencies 5 MHz, 15 MHz, 26 MHz and 36 MHz. The full curves show the theoretical absorption according to Bardeen, Cooper and Schrieffer, with a zero-temperature energy gap of 3·5 kT_c.

When the results of the measurements at 5 MHz, 15 MHz and 26 MHz for the (110) single crystal are plotted in the same way, the graphs are identical with those for the (100) single crystal. The results show a very good agreement with the BCS theory, up to 0·8 T_c. There are, however, small deviations at higher temperatures.

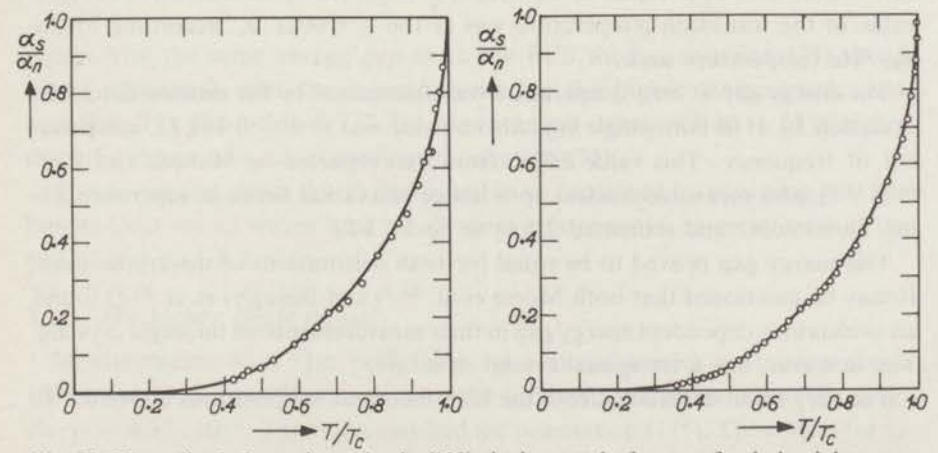

Fig. 20. Normalized absorption α_s/α_n in (100) single crystal of zone-refined aluminium as a function of T/T_c for $\nu = 5$ MHz. The full curve is the theoretical curve according to BCS.
Fig. 21. Normalized absorption in (100) single crystal for $\nu = 15$ MHz.

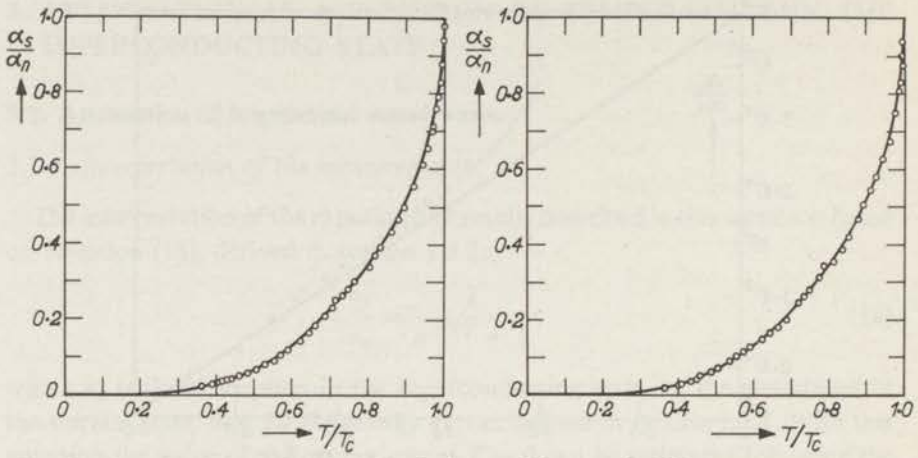

Fig. 22. Normalized absorption in (100) single crystal for $\nu = 26$ MHz.
Fig. 23. Normalized absorption in (100) single crystal for $\nu = 36$ MHz.

The similarity of the graphs showing α_s/α_n as a function of T/T_c for all frequencies, is in agreement with a theoretical work by Tsuneto [61,3]). He gave a general treatment of ultrasonic absorption in superconductors on the basis of the BCS theory, and showed that for longitudinal sound waves in superconductors equation (18) may be expected to hold for all experimentally available values of the product of sound wave number and mean free path of the conduction electrons.

For the (100) single crystal the values of α_n are 1·20 db/cm at 5 MHz, 4·9 db/cm at 15 MHz, 9·2 db/cm at 26 MHz and 13·1 db/cm at 36 MHz. For the (110) single crystal the values of α_n are 0·92 db/cm at 5 MHz, 5·05 db/cm at 15 MHz and 11·0 db/cm at 26 MHz *). For both specimens the measured value of the transition temperature was (1·166 $\pm$ 0·002) °K, according to the T_{62} ^{3}He temperature scale.

The energy gap at zero temperature was determined by the method described in section 3.1.1. In both single crystals its value was (3·5 $\pm$ 0·1) kT_c, independent of frequency. This value differs from that reported by Masuda and Redfield [62,6]), who measured nuclear spin-lattice relaxation times in superconducting aluminium, and estimated $2\Delta(0)$ to be 3·2 kT_c.

The energy gap proved to be equal for both orientations of the crystal axes. It may be mentioned that both Morse et al. [59,5]) and Bezuglyĭ et al. [61,2]) found an orientation-dependent energy gap in their measurements on tin single crystals. Tin, however, has a tetragonal crystal structure.

The very small deviations from the BCS theory at temperatures above 0·8 T_c

*) Some of the measurements described in [62,5]) were repeated after modification of the Arenberg amplifier to make it more sensitive.

must now be discussed. Similar, but somewhat larger deviations were observed with tin and indium; see figure 7. A possible explanation for the deviations is that the dependence of Δ on the temperature as proposed in the BCS theory needs a correction. We therefore tried another expression, suggested by Buckingham [56,7] [57,1]), for Δ as a function of temperature, valid for temperatures near T_c only, namely

$$2\Delta = 3{\cdot}2\, kT_c\, [1 - (T/T_c)]^{\frac{1}{2}} . \tag{21}$$

Combining this expression with equation (18) gives reasonably good agreement with the measurements on aluminium at $T > 0{\cdot}9\ T_c$, but too low values at lower temperatures.

We also tried another expression for the dependence of the absorption on the energy gap, using the energy gap proposed in the BCS theory. Pokrovskii [61,5]) has given a theoretical treatment of ultrasonic absorption in superconductors for different directions of the sound waves with respect to the crystal axes. At higher temperatures α_s/α_n is stated to depend on Δ in the same way as in the BCS theory. Pokrovskii found the following expression for temperatures well below T_c:

$$\frac{\alpha_s}{\alpha_n} = \sqrt{T/T_c}\, e^{-\Delta/kT} . \tag{22}$$

This formula yields much too low values for α_s; it gives no agreement at all with the experimental results.

Finally, because of the resemblance between equations (18) and (22) we tried combining them to give

$$\frac{\alpha_s}{\alpha_n} = \frac{2\sqrt{T/T_c}}{e^{\Delta/kT} + 1} . \tag{23}$$

Again with the same energy gap as in the BCS theory, equation (23) shows better agreement with the measurements for the higher temperatures than equation (18). But below $0{\cdot}7\ T_c$ the experimental values are 20 to 25 % higher than the values of α_s/α_n according to equation (23).

The deviations above $0{\cdot}9\ T_c$ can possibly be explained by assuming that the longitudinal sound waves have small shear components, as mentioned at the end of section 1.3.3.

3.1.3. *The impure single crystal*

Measurements were also performed on a single crystal containing about 100 p.p.m. of impurities *) and with the following resistance ratio: $R_{4{\cdot}24\ ^\circ K}/R_{0\ ^\circ C} = 4{\cdot}37\ .\ 10^{-3}$. The main axis had the orientation (115). The results for α_n

*) I wish to thank Dr. C. J. Berghout, of Philips' Research Laboratories, for preparing the single crystal.

over a large frequency range are given in table I, while in figure 24 the values of α_n are plotted against the square of the frequency. We see that α_n is proportional to the square of the frequency from 5·1 to 116 MHz, which is due to the relatively high concentration of impurities.

At all frequencies the same variation of α_s/α_n with T/T_c was found as for the very pure single crystals. The energy gap at zero temperature was determined as described in section 3.1.1. Its value was 3·4 to 3·5 kT_c, independent of frequency.

TABLE I

Normal-state absorption as a function of frequency for longitudinal sound waves in an impure single crystal of aluminium

specimen length	29·57 mm										15·84 mm		
ν (MHz)	5·1	15·1	25·1	35·3	45·4	56	66	76	86	96	96	106	116
α_n (db/cm)	0·03	0·24	0·66	1·25	2·07	3·00	4·41	5·56	7·05	8·89	8·99	10·75	12·98

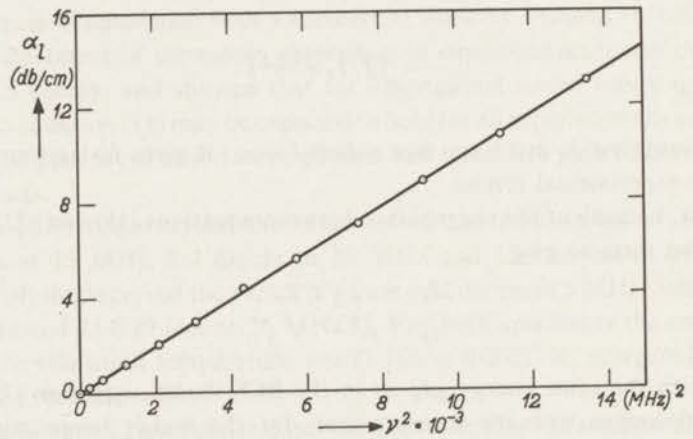

Fig. 24. α_n in impure single crystal as a function of ν^2 for longitudinal sound waves.

3.1.4. *The impure polycrystalline specimen*

Similar measurements were performed on a polycrystalline specimen containing about 100 p.p.m. of impurities. The results for α_n are presented in table II. In figure 25 the values of α_n are plotted against the square of the frequency, again showing a linear relationship throughout the whole frequency range. The graphs showing α_s/α_n as a function of T/T_c for longitudinal sound waves are identical with those of the other specimens at all frequencies. The energy gap at zero temperature was again found to be 3·4 to 3·5 kT_c for all frequencies.

TABLE II

Normal-state absorption as a function of frequency for longitudinal sound waves in a polycrystalline specimen of aluminium, specimen length 18·25 mm

ν (MHz)	5·0	15·0	25·0	35·2	45·2	55·3	66	76
α_n (db/cm)	0·03	0·20	0·74	1·49	2·34	3·66	4·96	6·87

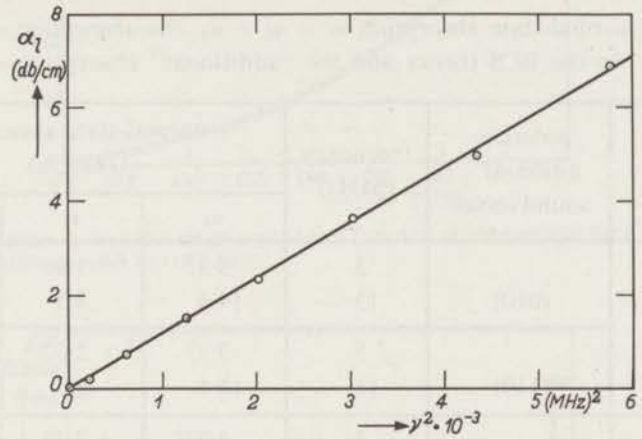

Fig. 25. α_n in polycrystalline specimen as a function of ν^2 for longitudinal sound waves.

3.2. Attenuation of shear sound waves

3.2.1. *The single crystals of zone-refined aluminium* [63,4])

General remarks

Shear-wave measurements were performed on the same single crystals as those mentioned in section 3.1.2. We used *Y*-cut quartz crystals with a main resonance frequency of 2·5 and 5 MHz for transmitting and for detecting the sound waves. The positions of their *X*-axes had been determined by means of X-ray reflection. The quartz crystals were oriented by hand with their *X*-axes parallel to each of the main crystallographic axes of the specimens in turn, with an accuracy of about 2°.

The high purity of the specimens causes a rather large shear-wave attenuation. As the attenuation was even larger than for longitudinal waves, measurements at higher frequencies than 15 MHz were not performed above the transition temperature, except in the (110) single crystal for a sound polarization parallel to the cubic (100) axis. This led to an attenuation which was somewhat smaller than for the other shear-wave measurements, frequency for frequency. The attenuation for a sound polarization of (100) was measured in the (110) single crystal at a large number of frequencies varying from 2·5 to 25·2 MHz. All

other measurements were performed only at 5 MHz and at 15 MHz, namely in the (110) single crystal with sound-wave polarization parallel to the cubic (101) axis and to the (111) axis, and in the (100) single crystal with polarization parallel to the (110) axis, to the (010) axis and with the polarization direction chosen at random.

TABLE III

The total normal-state absorption $\alpha_t = \alpha_1 + \alpha_2$, the absorption α_1 according to the BCS theory and the "additional" absorption α_2

single crystal	polarization of sound waves	frequency (MHz)	normal-state absorption (db/cm)		
			α_t	α_1	α_2
(100)	(010)	5	3·33	1·96	1·37
		15	14·4	4·5	9·9
	(110)	5	3·37	2·02	1·35
		15	14·4	4·3	10·1
(110)	(111)	5	4·02	2·73	1·29
		15	11·6	6·4	5·2
	(101)	5	4·58	3·80	0·78
		15	18·3	11·7	6·6
	(100)	2·5	0·59	0·56	0·03
		5·1	2·58	1·96	0·62
		7·5	5·0	2·8	2·1
		12·5	9·1	4·1	5·0
		15·1	10·4	4·5	5·9
		17·5	12·3	4·9	7·4
		22·4	15·5	5·7	9·8
		25·2	18·3	6·4	11·9

The values of the normal-state absorption α_t as obtained from the measurements and corrected for non-electronic attenuation are given in table III. All the measured values had an accuracy of about 5%, except for those at 2·5 MHz, where the accuracy was somewhat less.

Measurements on the superconducting state showed that the attenuation dropped very sharply just below the transition temperature T_c and then decreased much more gradually as the temperature was lowered still further. Some of the absorption-temperature curves for the (100) single crystal are shown in

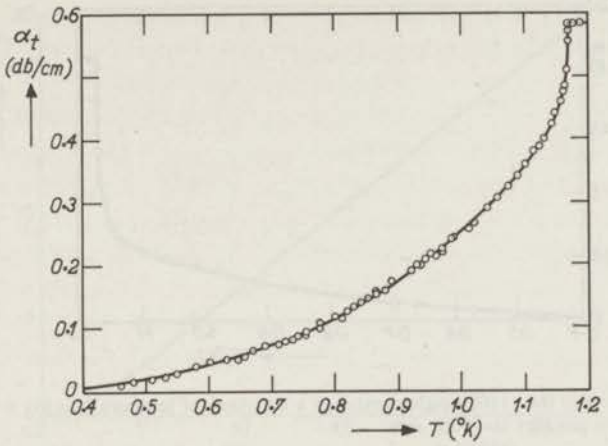

Fig. 26. Absorption in the (110) single crystal as a function of temperature for $\nu = 2\frac{1}{2}$ MHz, sound polarization parallel to (100) axis.

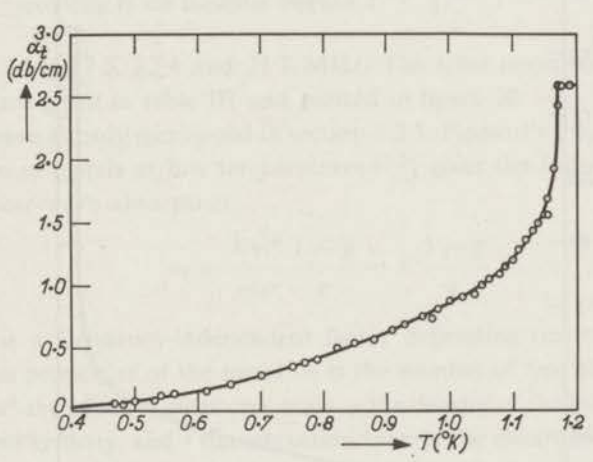

Fig. 27. Absorption in the (110) single crystal as a function of temperature for $\nu = 5$ MHz, sound polarization parallel to (100) axis.

figures 26 to 29. It will be seen that the form of these curves is highly frequency-dependent.

Measurements on the (100) single crystal show that the curves representing the absorption as a function of the temperature are identical for both sound-wave polarizations, within the limits of the experimental accuracy. Measurements at 5 MHz and at 15 MHz were performed at different sound-wave polarizations. Only the results of those measurements where the direction of the polarization was accurately determined are given in table III.

For the (110) single crystal there is an obvious anisotropy for different polarization directions. As this anisotropy was also observed at room temper-

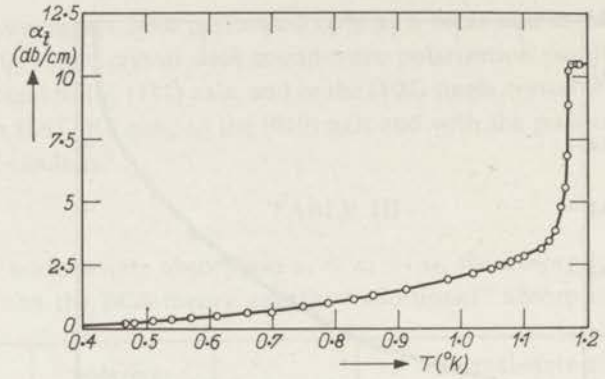

Fig. 28. Absorption in the (110) single crystal as a function of temperature for $\nu = 15$ MHz, sound polarization parallel to (100) axis.

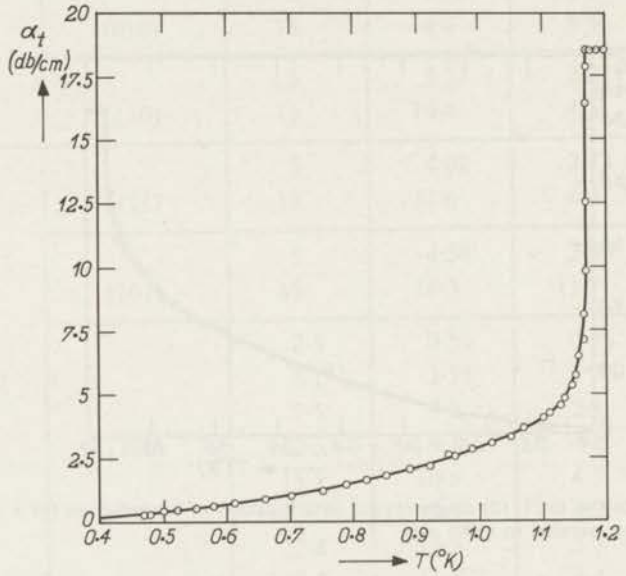

Fig. 29. Absorption in the (110) single crystal as a function of temperature for $\nu = 25$ MHz, sound polarization parallel to (100) axis.

ature, where the mean free path of the conduction electrons is relatively small, it is apparently connected with the lattice structure. In the (100) single crystal this kind of anisotropy was not observed at room temperature.

The normal state

The attenuation in the (110) single crystal with sound polarization parallel to the (100) axis was measured at eight different frequencies, namely at 2·5, 5·1,

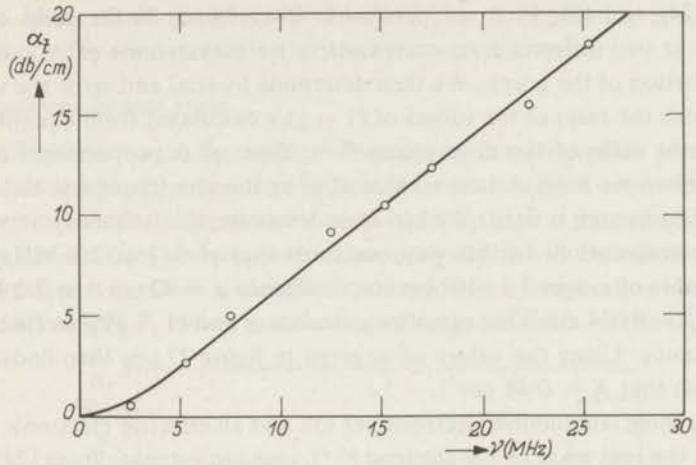

Fig. 30. Total normal-state absorption in the (110) single crystal as a function of frequency, sound polarization parallel to (100) axis. The full curve gives the absorption as a function of frequency according to the theory of Pippard.

7·5, 12·5, 15·1, 17·5, 22·4 and 25·2 MHz. The total normal-state absorption values α_t are given in table III and plotted in figure 30.

As we have already mentioned in section 1.2.3, Pippard's theory of ultrasonic absorption in metals at low temperatures [55,1]) gives the following expression for the shear-wave absorption:

$$\alpha_t = \frac{Nm^*}{\rho c_t \tau} \frac{1-g}{g} = K \frac{1-g}{g}, \tag{24}$$

where K is a frequency-independent factor depending on the electrical and mechanical properties of the metal, N is the number of free electrons per unit volume, m^* the effective electronic mass, ρ the density of the metal, c_t the transverse sound velocity, and τ the relaxation time of the electrons. The frequency-dependent part of the absorption is contained in the factor $(1-g)/g$, where

$$g = \frac{3}{2(q\bar{l})^2} \left\{ \frac{(q\bar{l})^2 + 1}{q\bar{l}} \arctan(q\bar{l}) - 1 \right\}. \tag{9}$$

Here q represents the ultrasonic wave number, which is equal to 2π divided by the wavelength of the sound, and $\bar{l}$ is the mean free path of the conduction electrons.

Pippard distinguishes between two frequency ranges, above and below the frequency for which $q\bar{l} = 1$. Equations (24) and (9) show that α_t is proportional to the square of the frequency for $q\bar{l} < 1$, and to the frequency itself for $q\bar{l} > 1$. It is clear from figure 30 that the measurements from 2·5 to 25·2 MHz were performed in the range where $q\bar{l} > 1$.

The frequency at which $q\bar{l} = 1$ can be calculated as follows with the aid of

equations (24) and (9). First we determine from figure 30 the ratio of the absorptions at two different frequencies where we may assume $q\bar{l} > 1$, i.e. on the linear portion of the graph. We then determine by trial and error the values of $q\bar{l}$ for which the ratio of the values of $(1-g)/g$ calculated from equation (9) is equal to the ratio of the absorptions [63,5]). Since $q\bar{l}$ is proportional to the frequency, when we have chosen a value of $q\bar{l}$ at the one frequency, the value at the other frequency is fixed. We can now determine the frequency at which $q\bar{l} = 1$ by extrapolation. In this way one finds that $q\bar{l} = 1$ at 2·2 MHz. The measured value of c_t was $3{\cdot}3 \cdot 10^5$ cm sec^{-1}; whence $q = 42$ cm^{-1} at 2·2 MHz. This yields $\bar{l} = 0{\cdot}024$ cm. One can then calculate g and $(1-g)/g$ as functions of the frequency. Using the values of α_t given in figure 27 one then finds from equation (24) that $K = 0{\cdot}48$ cm^{-1}.

Assuming three conduction electrons per ion and an effective electronic mass of 1·6 times the real mass of the electron [55,6]), one can estimate from (24) that the relaxation time τ is $6{\cdot}1 \cdot 10^{-10}$ sec. This leads to the Fermi velocity $v_F = \bar{l}/\tau = 0{\cdot}39 \cdot 10^8$ cm sec^{-1}. The Fermi velocity can be evaluated in a more straightforward way from the slope of the straight part of the absorption-frequency curve, which is equal to $(8Nm^*v_F)/3\rho c_t^2$. This leads to the same value for v_F, within the limits of the experimental accuracy.

One can also calculate the Fermi velocity theoretically. For an isotropic metal with a spherical Fermi surface the ground-state Fermi energy is

$$E_F = \frac{h^2}{2\,m^*}\left(\frac{3}{8\,\pi}\frac{N}{}\right)^{2/3}. \qquad (4)$$

This equation leads to a Fermi energy of $11{\cdot}7 \cdot 10^{-12}$ erg, and hence a Fermi velocity of $1{\cdot}27 \cdot 10^8$ cm sec^{-1}.

A part of the discrepancy between the experimental and theoretical values may be attributed to the fact that the attenuation in the (110) single crystal with sound polarization parallel to the (100) axis is considerably lower than the other measured attenuations.

According to Pippard's theory the limiting value of the ratio of transverse-wave absorption to longitudinal-wave absorption at low temperatures, for $q\bar{l} \gg 1$, is

$$\frac{\alpha_t}{\alpha_l} = \frac{8}{\pi^2}\left(\frac{c_l}{c_t}\right)^2. \qquad (11)$$

As we measured $c_l = 6{\cdot}3 \cdot 10^5$ cm sec^{-1} and $c_t = 3{\cdot}3 \cdot 10^5$ cm sec^{-1}, we may expect the limiting value of α_t/α_l to be $2{\cdot}9_5$.

In the (100) single crystal the value of this ratio is 2·8 at 5 MHz and 2·9 at 15 MHz. The agreement with the theory is thus very good. For the (110) single crystal the discrepancy between theory and experiment is much larger: the values of the ratio obtained from attenuation measurements are partly higher and

partly lower than the theoretical value. This is apparently connected with anisotropy for the attenuation of transverse sound waves.

The superconducting state

The explanation of the sudden decrease in the absorption just below the transition temperature has been indicated in section 1.3.3, where it was shown that the curves for shear waves can be split up into a part obeying the BCS theory for electron-phonon interaction and which will be called α_1, and an additional part α_2 which is cancelled out rapidly in a temperature range between T_c and about 0·98 T_c owing to screening of magnetic fields by the supercurrents.

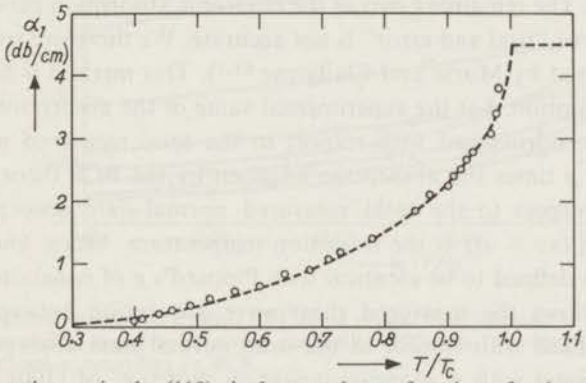

Fig. 31. Absorption α_1 in the (110) single crystal as a function of reduced temperature for $\nu = 15$ MHz, sound polarization parallel to (100) axis. The broken curve is the theoretical curve according to BCS normalized with respect to α_1 for the normal state.

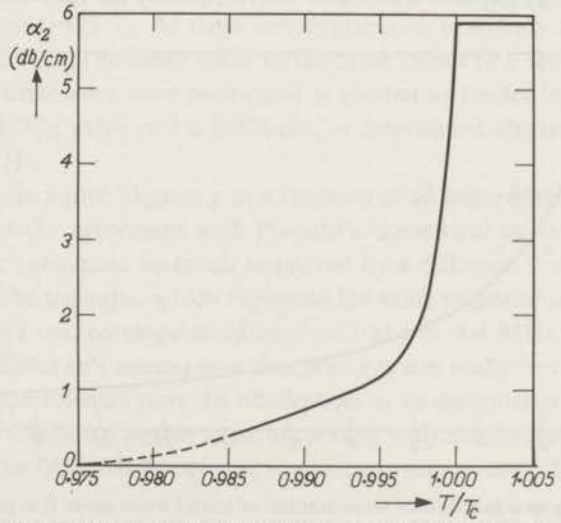

Fig. 32. Absorption α_2 in the (110) single crystal as a function of reduced temperature for $\nu = 15$ MHz, sound polarization parallel to (100) axis. This curve is obtained by subtracting the absorption of figure 31 from the total absorption, given in figure 28.

The variation of α_2 with the temperature, determined as described below, is shown in figure 32 for 15 MHz sound in the (110) single crystal, with the sound-wave polarization parallel to the (100) axis, while figure 31 shows α_1 for the same case. The theoretical BCS curve for a zero-temperature energy gap of $3{\cdot}5\ kT_c$ is given by the broken curve. The curves of figures 31 and 32 are derived from figure 28.

There are two possible methods for splitting up the absorption curves into α_1 and α_2. The first one is the method of "trial and error", in which one determines the additive constant which gives the best fit between the BCS curve (α_1) and the experimental points over the whole temperature range below T_c, as described in section 3.1.1. The remaining part of the electronic absorption curve is then α_2.

This method of "trial and error" is not accurate. We therefore tried a second method, proposed by Morse and Claiborne [62,1]). This method is based on the following assumption. Let the experimental value of the absorption just below the steep drop, normalized with respect to the total measured normal-state absorption, be p times the absorption as given by the BCS theory, also normalized with respect to the total measured normal-state absorption. Then p is equal to $\alpha_1/(\alpha_1 + \alpha_2)$ at the transition temperature. Morse and Claiborne assumed p thus defined to be identical with Pippard's g of equation (9).

Figure 34 shows the measured shear-wave absorption between 0·95 and 0·99 T_c normalized with respect to the total normal-state absorption for the (110) single crystal with a sound-polarization direction of (100), for all frequencies at which measurements were performed. The broken curve gives the theoretical normalized absorption according to the BCS theory, with a zero-temperature energy gap of $3{\cdot}5\ kT_c$. For each frequency the ratio of the measured

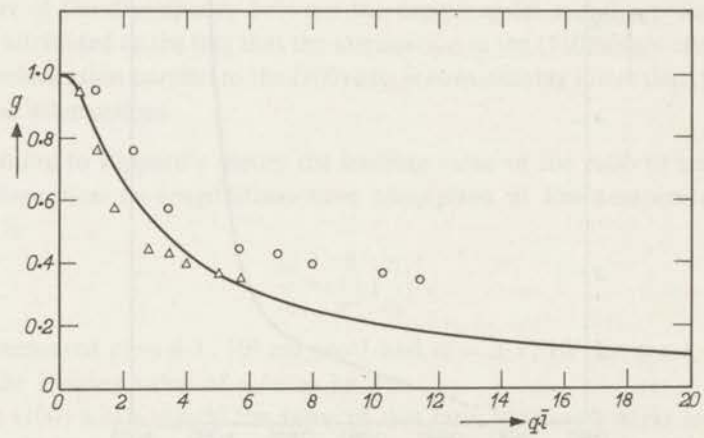

Fig. 33. Pippard's g as a function of wave number of sound times mean free path of electrons. The circles represent values of Morse and Claiborne's p for the (110) single crystal, sound polarization parallel to (100) axis, on the assumption that $q\bar{l} = 1$ for $\nu = 2{\cdot}2$ MHz. The triangles correspond to the same absorption values, but with $q\bar{l} = 1$ for $\nu = 4{\cdot}4$ MHz.

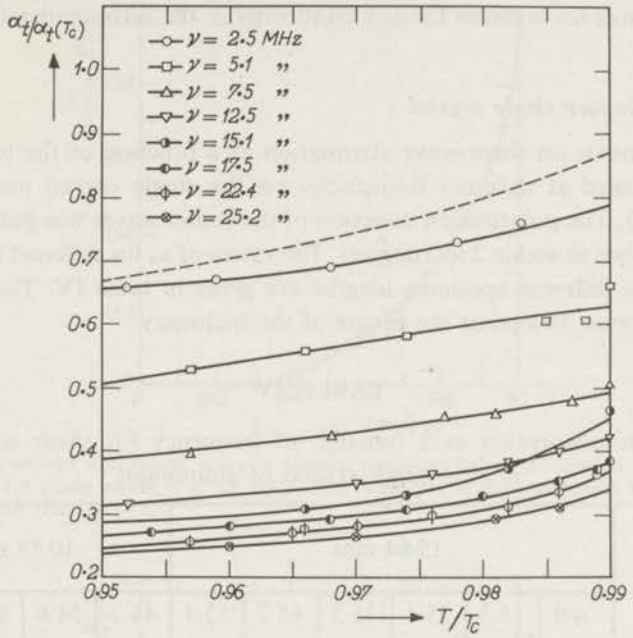

Fig. 34. Normalized absorption in the (110) single crystal as a function of temperature near T_c at eight frequencies, sound polarization parallel to (100) axis. The broken curve gives the theoretical absorption according to BCS.

normalized absorption to the normalized absorption according to the BCS theory was calculated at three different temperatures just below T_c, namely at 0·955, 0·965 and 0·975 T_c. At these temperatures α_2 is already zero, as may be seen from figure 32. The mean value of the three values of p for each frequency at which measurements were performed is plotted as circles in figure 33, as a function of $q\bar{l}$. The value of $\bar{l}$ is 0·024 cm, as determined above, so that $q\bar{l} = 1$ at $\nu = 2{\cdot}2$ MHz.

The full line in figure 33 gives g as a function of $q\bar{l}$, according to equation (9). It is clear that the agreement with Pippard's theoretical curve for g is rather poor, nor can agreement be much improved by a different choice of $\bar{l}$. This is illustrated by the triangles, which represent the same values of p plotted against $q\bar{l}$ for $\bar{l} = 0{\cdot}012$ cm, corresponding to $q\bar{l} = 1$ at $\nu = 4{\cdot}4$ MHz. It is clear that Morse and Claiborne's assumption that $p = g$ is not really justified. Nevertheless, for all experimental runs the absorption α_1 as determined by the method of Morse and Claiborne agrees quite accurately with the theoretical absorption according to the BCS theory over the whole temperature range. This is illustrated in figure 31.

The zero-temperature energy gap was determined from the experimental values of α_1 as described in section 3.1.1, and was found to be 3·4 to 3·5 times

kT_c. There was no evidence for any anisotropy of the zero-temperature energy gap.

3.2.2. *The impure single crystal*

Measurements on shear-wave attenuation as a function of the temperature were performed at different frequencies on the single crystal mentioned in section 3.1.3. The polarization direction of the sound waves was parallel to the (100) cubic axis to within 2 to 3 degrees. The values of α_n for different frequencies and for two different specimen lengths are given in table IV. They are also plotted in figure 35 against the square of the frequency.

TABLE IV

Normal-state absorption as a function of frequency for shear waves in an impure single crystal of aluminium

specimen length	15·84 mm						10·88 mm			
ν (MHz)	4·9	15·3	25·4	35·5	45·2	55·4	44·7	54·6	64·4	74
α_n (db/cm)	0·11	1·03	2·80	5·24	8·80	13·06	8·80	13·01	17·8	21·8

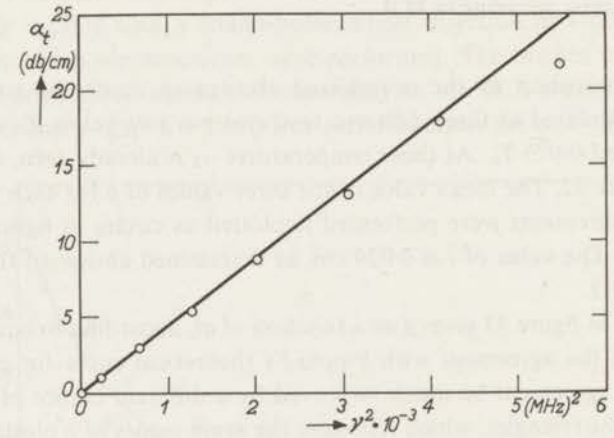

Fig. 35. α_n in impure single crystal as a function of ν^2 for shear waves.

At frequencies up to 45 MHz the graphs of normalized shear-wave absorption against normalized temperature satisfy the classical BCS theory. At frequencies of 55, 64 and 74 MHz the absorption decreased more at the transition temperature than according to the BCS theory. Keeping to the notation of α_1 and α_2 used in section 3.2.1, we found that at 55 MHz α_2 is approximately 5% of the total normal-state absorption and at 64 and 74 MHz approximately 10%. In

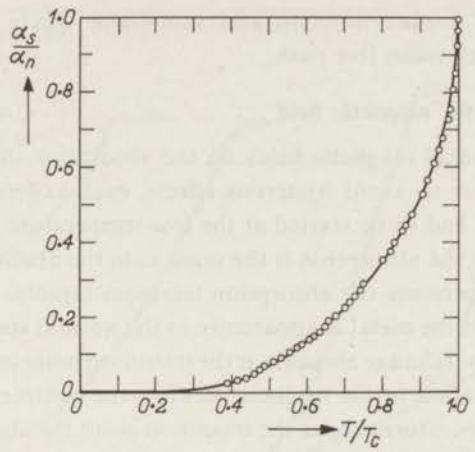

Fig. 36. Normalized absorption α_s/α_n in impure single crystal as a function of normalized temperature for shear waves, $\nu = 25$ MHz. The full curve is the theoretical BCS curve, on the assumption that $\alpha_2 = 0$.

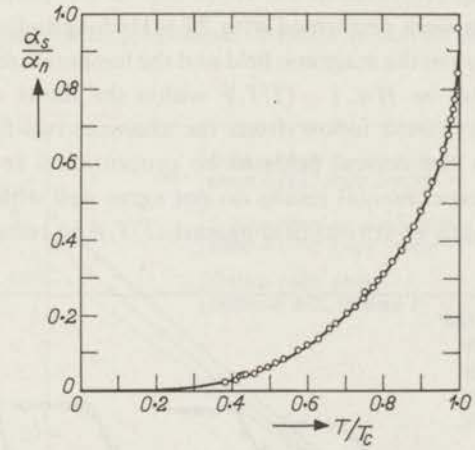

Fig. 37. Normalized absorption α_s/α_n in impure single crystal as a function of normalized temperature for shear waves, $\nu = 64$ MHz. The full curve is the theoretical BCS curve, on the assumption that $\alpha_2 = 0{\cdot}10\ \alpha_n$.

figure 36 the normalized absorption for 25-MHz shear waves is plotted against the normalized temperature. The full line is the theoretical BCS curve ($\alpha_2 = 0$). Figure 37 shows the normalized absorption plotted against normalized temperature for 64 MHz. The full line here is the theoretical BCS curve for $\alpha_1 = 0{\cdot}90\ \alpha_n$.

From the measurements described in this section it is obvious that for sufficiently small values of $q\bar{l}$ the steep drop in the absorption curve disappears, and the absorption as a function of the temperature obeys the classical BCS theory in the whole temperature range below T_c [63,6]). This agrees with the results by

Levy et al. [62,7]) on impure niobium and vanadium, where the conduction electrons have a small mean free path.

3.3. Dependence on the magnetic field

The influence of small magnetic fields on the absorption of ultrasound was also studied. In order to avoid hysteresis effects, each experimental run at a small magnetic field had to be started at the low-temperature side. The curves indicate that initially the absorption is the same as in the absence of a field, but above a certain temperature the absorption increases rapidly, until a temperature is reached where the metal is apparently in the normal state. The fact that the absorption does not change abruptly at the transition point must be attributed to a gradual penetration of the magnetic flux into the specimen with increasing temperature. At temperatures above the transition point the absorption remains constant. The absorption for the normal-state metal is not exactly equal to the absorption in the absence of a magnetic field; there is a small field dependence.

Figures 38 and 39 show the results of some experimental runs for the pure single crystals at magnetic fields of 24, 41, 68 and 83 Oe, parallel to the sound beam. Measurements were performed with 25-MHz longitudinal sound waves. The relationship between the magnetic field and the temperature at the transition point was found to be $H \propto 1 - (T/T_c)^2$ within the limits of our accuracy. This proportionality would follow from the classical two-fluid model. The BCS theory predicts the critical fields to be proportional to $1 - 1{\cdot}07(T/T_c)^2$ well below T_c. The experimental results do not agree well with this prediction.

Supposing the graphs of critical field against $(T/T_c)^2$ to remain straight lines

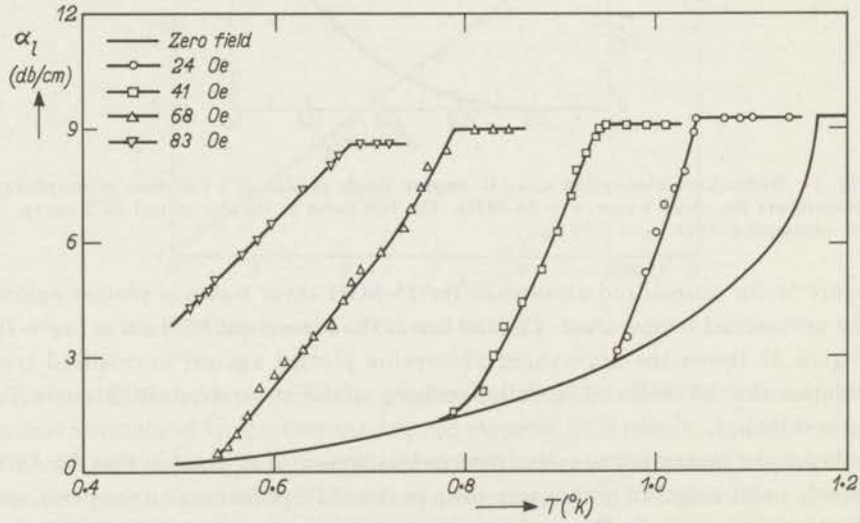

Fig. 38. Absorption of 25-MHz longitudinal sound waves in (100) single crystal at constant magnetic fields.

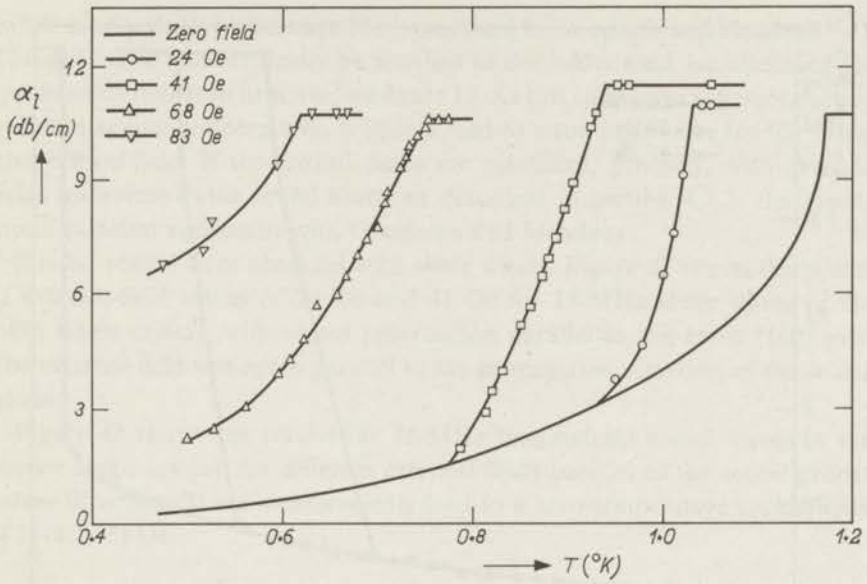

Fig. 39. Absorption of 25-MHz longitudinal sound waves in (110) single crystal at constant magnetic fields.

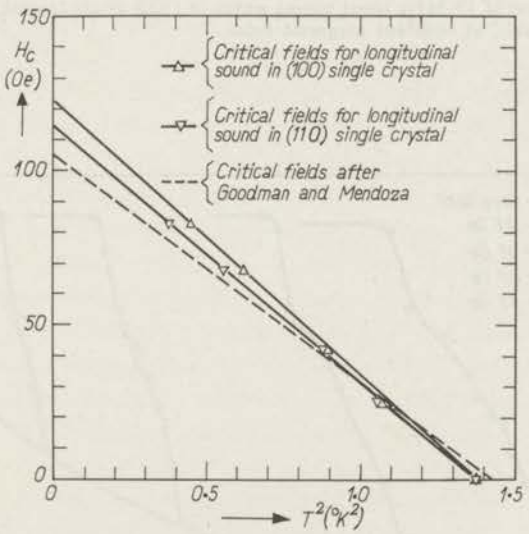

Fig. 40. Critical field as a function of temperature.

below 0·4 °K, one can extrapolate the critical field to zero temperature. This is shown in figure 40, for longitudinal-sound absorption in the pure single crystals. This extrapolation yields a zero-temperature critical field of (123 $\pm$ 5) Oe for the (100) single crystal and (114 $\pm$ 5) Oe for the (110) single crystal. These

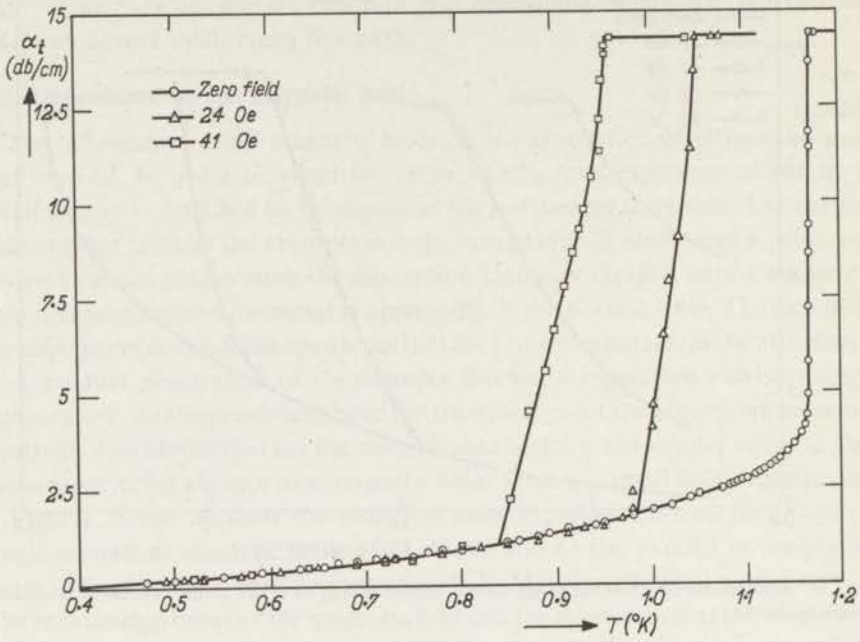

Fig. 41. Absorption of 15-MHz shear sound waves in (100) single crystal, sound polarization parallel to (110) axis, at constant magnetic fields.

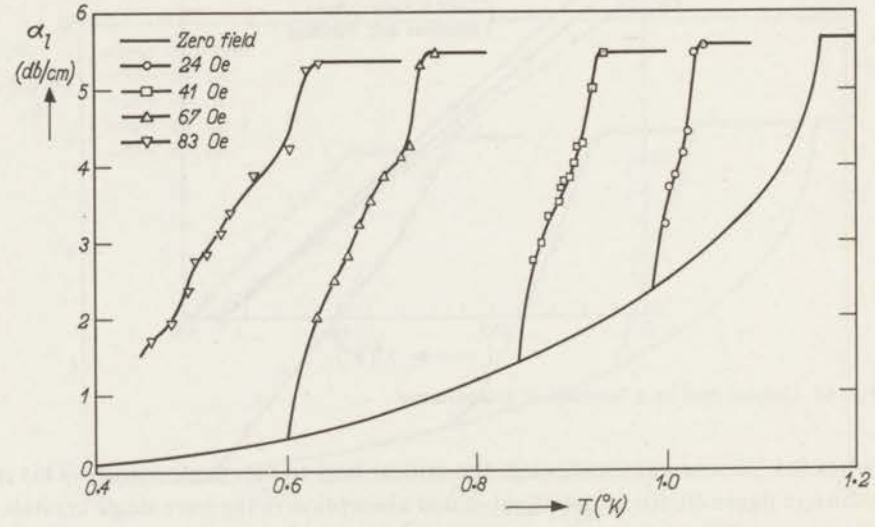

Fig. 42. Absorption of 76-MHz longitudinal sound waves in impure single crystal at constant magnetic fields.

values are decidedly higher than 106 Oe as found by Goodman and Mendoza [51,1]). This difference must evidently be ascribed to the solder used for attaching the specimen container to its cover, see figure 13. As this solder was superconducting at liquid-helium temperatures, it should lead to a too high value for the measured critical field. If the critical fields are measured, however, with external fields transverse to the sound beam, as described in section 4.2.3, the results are in excellent agreement with Goodman and Mendoza.

Similar results were obtained with shear waves. Figure 41 shows the results at external-field values of 24 Oe and 41 Oe for 15-MHz shear waves in the (100) single crystal, with sound polarization parallel to the cubic (110) axis. The external field was again parallel to the propagation direction of the sound waves.

Figure 42 shows the results for 76-MHz longitudinal sound waves in the impure single crystal, for different external fields parallel to the sound-propagation direction. These measurements lead to a zero-temperature critical field of (114 ± 5) Oe.

4. ULTRASONIC MEASUREMENTS DURING PHASE TRANSITIONS IN ALUMINIUM

4.1. Some considerations on phase transitions

4.1.1. *The intermediate state*

The magnetic-flux pattern in and around a body placed in an external magnetic field is determined by the shape of the body as well as by the magnetic permeability μ.

In the case of ellipsoids the influence of the shape is readily described by means of the demagnetization factor D. The value of this demagnetization factor is between zero and unity. For an infinitely long cylinder parallel to the external field this value is zero, for an infinitely long cylinder perpendicular to the external field $\frac{1}{2}$ and for a sphere $\frac{1}{3}$.

A superconducting specimen in an external magnetic field everywhere around the specimen smaller than the critical field H_c, results in a flux pattern which is exclusively governed by the shape of the specimen, μ being zero. The magnetic induction $B = \mu_0 (H_i + M)$ is thus also zero everywhere inside the specimen, whence the magnetization M is equal to minus the "internal field" H_i. Since $H_i = H_e - DM$, where H_e is the undistorted external field, $H_i = H_e/(1 - D)$. As the external field increases, magnetic flux will therefore start to penetrate into the specimen at $H_e = H_c (1 - D)$. Penetration starts where the lines of force are densest. When H_e increases further to some value below the critical field, it will not be possible for the specimen to remain entirely in the superconducting state, nor will the whole specimen become normally conducting. A superconducting core surrounded by a normally conducting shell is easily shown [60,5]) to be unstable as follows. At the interface between the superconducting phase and the normal phase the magnetic field must be equal to H_c, and the interface lines of force are tangential to the surface. If the interface were convex with respect to the normal phase, the magnetic equipotential surfaces would diverge from the boundary into the normal region, and the field would decrease in the normal region to values below H_c, leading to a contradiction. If, on the other hand, the interface were concave with respect to the normal phase, then the lines of force would be bent at the interface, leading locally to an infinite magnetic field. But such an infinite magnetic field would lead to the rapid conversion of superconducting into normally conducting material.

It has been shown both experimentally and theoretically that a stable structure is that where the entire specimen is subdivided into normal regions with $H_i = H_c$ and $B = \mu H_c$, alternating with superconducting regions having $B = 0$. A specimen having such a structure is said to be in the intermediate state.

Some investigators have provided information about the structure of the intermediate state, and about shifting of the phase boundaries when the external magnetic field is suddenly altered. Schawlow [56,8]) measured domain spacing in several intermediate-state tin and vanadium specimens. He used a photographic method, the superconducting domains at the surface being indicated by means of niobium powder. Similar investigations were performed at the same time by Balashova and Sharvin [57,6]) on tin spheres, using nickel powder for indicating the normal regions. For external fields well below H_c they observed a detailed structure with corrugated superconducting laminae. This phenomenon of corrugation was observed more extensively by Faber [58,4]) on thin aluminium plates perpendicular to the external magnetic field. Faber also derived an expression for the interphase surface energy in terms of the thickness of the plate and the distance between domains. Applying this expression to his measurements he estimated that the surface energy for aluminium is seven times that of tin [55,7]).

Faber showed by his experiments on thin aluminium plates in the temperature range between $0{\cdot}85\,T_c$ and T_c that the corrugations mentioned above exist only at $H_e/H_c < 0{\cdot}6$. As in our experiments the external magnetic field did not penetrate into the aluminium specimen at $H_e/H_c < 0{\cdot}6$, those corrugations were not expected to occur in our specimen.

Faber also studied the flux displacement due to the shifting of the phase boundaries during the transition from the normal to the superconducting state and vice versa in tin rods, using a ballistic method [52,1]) [53,3]) [54,2]). This method is also useful for studying the quantity of displaced flux for the transition to and from the intermediate state and phase-propagation velocities. Hardly any information can be obtained, however, about the geometry of the structure.

It is rather uncertain whether phase transitions can be investigated correctly in aluminium by powder photography when the external fields are of the order of the critical field, as this critical field is rather low: the niobium powder which indicates the superconducting regions may well lag behind when the external field is altered [58,4]).

One may conclude that none of the methods mentioned above is adequate for providing a complete three-dimensional picture of the structure of the intermediate state and of the shifting of phase boundaries. The photographic methods give a picture of the structure at the surface of the specimen, whereas the ballistic method gives information about phase-transition times. Time-dependent ultrasonic attenuation measurements provide the same information about phase-transition times as the ballistic method, combined with some information about the structure of the specimen. Up till now the only paper on phase-transition measurements by using ultrasonic attenuation was that by Chopra and Hutchison [59,1]). They performed measurements on aluminium containing 60 p.p.m. of impurities at magnetic fields larger than the critical field, leading to values

of the phase-transition time for different values of H_e/H_c. It has been proved that the times of transition from the superconducting to the normal phase are proportional to the electrical conductivity of the normal phase. These transition times measured by Chopra and Hutchison were therefore much shorter than for our very pure specimen of about the same dimensions. These were of the order of one second. The transitions from the normal to the superconducting phase took somewhat longer, namely about 10 sec.

The measurements mentioned above together with theoretical considerations led to the following simplified model of the intermediate state for a specimen with a positive interphase surface energy, for $H_e > 0{\cdot}6\ H_c$. The superconducting regions run as laminae or cylinders through a normally conducting bulk, and they are oriented parallel to the external magnetic field. In the superconducting regions $B = 0$ and in the normally conducting part of the metal $B = \mu H_c$ and the internal field is equal to H_c. In a plane perpendicular to the external field the equilibrium ratio of the sum of the superconducting areas to the total area is equal to $(H_c - H_e)/DH_c$, as is readily verified; D is the demagnetization factor defined above. The spacing of the superconducting regions is essentially determined by the interphase surface energy. Pure aluminium for instance, with a large surface energy, has a relatively large spacing between the superconducting regions. For pure tin the surface energy, and also the spacing, are much less. The surface energy has been proved to diminish on addition of impurities. The fact that the spacing is also diminished by impurities has not yet been established by experiment.

4.1.2. *Supercooling*

The superconducting transition temperatures mentioned throughout this thesis are defined for the transition from the superconducting to the normal state, i.e. for increasing temperature. Similarly the critical fields are defined for increasing external magnetic fields. When a specimen is cooled at a small magnetic field through the transition point, the normal phase sometimes persists down to a temperature below the transition temperature for that external field. The same thing sometimes occurs when an external magnetic field larger than the critical field decreases continuously, at a constant temperature below the zero-field transition temperature. This phenomenon is called supercooling, both for decreasing temperature and for decreasing magnetic field. The lowest external field at which superconductivity appears when the external field is lowered at a fixed temperature is called the "nucleating field" H_l. The degree of supercooling is commonly defined as

$$\varphi = 1 - (H_l/H_c)^2 . \tag{25}$$

This phenomenon may be compared with the supercooling of a pure liquid below the freezing point. Both situations are analogous in so far as both in the

supercooled liquid and in the normal-state metal a metastable state apparently exists, below the superconducting transition temperature and below the critical field. This metastable state is replaced by a more highly ordered stable state by "phase-transition nuclei".

Nucleation of the superconducting phase has been assumed by Faber to originate at local flaws. The dimensions of the nuclei must initially be smaller than the largest possible range of interaction of a pair of superconducting electrons, the "coherence range". In order to induce propagation of the superconducting phase, a nucleus must however extend over a domain whose radius exceeds the coherence range [55,7] [55,8]). When the external magnetic field is lowered from a value greater than the critical field to a value less than the critical field, or when the temperature is lowered from above the transition temperature to below the transition temperature in the presence of a small magnetic field, growth from the nuclei is opposed by the fact that the energy gain due to ordering at the nuclei is initially less than the loss of magnetization energy by the expulsion of magnetic flux. At a small enough field or at a low enough temperature the nucleus starts to extend in space. The growth rate has not yet been given in a formula, but one can predict that the phase propagation will depend on the interphase surface energy Δ in the same way as for propagation of the superconducting phase along the surface of a pure normally-conducting body [54,2] [62,8]), namely $v \propto (\Delta - \lambda)^{-2}$, where λ is the penetration depth. The interphase surface energy for pure aluminium is very large compared to that for other pure metals, e.g. tin, thus accounting for the low phase-propagation velocities in pure aluminium compared to the results for tin [54,2]). Our experimental results for the phase-propagation velocities in pure aluminium will be discussed in section 4.2.

Faber [52,1]) proposed the following tentative formula for the degree of supercooling

$$\varphi = \Delta/z + n, \tag{26}$$

where Δ is the interphase surface energy divided by $\mu H_c^2/2$, z is related to the dimensions of the nucleus perpendicular to the magnetic field, and n depends on the demagnetization factor of the nucleus. Supercooling experiments by Faber on tin, indium and aluminium [52,1]) [57,7]) and by Cochran, Mapother and Mould on aluminium [56,9]) [58,5]) have shown that the degree of supercooling for aluminium exceeds by far the degree of supercooling for the two other metals. According to equation (26) these results are consistent with the fact that the interphase surface energy for aluminium is much larger than for both other metals.

Some supercooling occurred during the measurements described in sections 3.1 and 3.2. It proved to be necessary to start each experimental run on the low-

temperature side, because when the temperature of the aluminium specimens was lowered through the transition point a non-reproducible discontinuity in the attenuation was observed. The apparent transition temperature for decreasing temperatures proved to be about 0·01 °K lower than that found when the specimen was heated through the transition point. At temperatures more than 0·02 °K below the transition temperature the attenuation-temperature curve was reversible.

This effect is assumed to be caused by supercooling due to the magnetic field of the earth and to small stray fields from outside the equipment. It occurred both with the pure and with the less pure specimens. At the small external fields used in the experiments described in section 3.3, the supercooling effect was much more significant.

4.1.3. *Kinetics of phase transitions*

A simplified description will now be given of the transition from the superconducting phase to the normal phase for a cylindrical specimen under the influence of an external magnetic field. This description, based upon the eddy-current theory, was first given by Pippard [50,1]). He assumed that when an external field $H_e = H_c\,(1 + p)$ parallel to the axis of the specimen is switched on, a normally conducting sheet will very rapidly be formed at the surface, after which the superconducting core will shrink symmetrically and eventually vanish at the central axis. Pippard assumed in his calculations that p is small compared to unity. The internal field can therefore be put equal to H_c throughout the normal region without appreciable error. This assumption simplifies the calculations.

Let the radius of the specimen be s and the radius of the superconducting core r_0, then the magnetic flux contained in the normal material between the superconducting core and a cylinder of radius r is given by $\Phi = \pi\,(r^2 - r_0^2)\,\mu H_c$. As the core contracts, the induced electric field at radius r is given by $E(r) = -(\mathrm{d}\Phi/\mathrm{d}t)/2\pi r$. This electric field causes an eddy current whose density at radius r is given by $J(r) = \sigma E(r)$. Now Maxwell's equations state that curl $H = J$. Transforming to cylindrical coordinates and integrating we find $\int_{r_0}^{s} J\mathrm{d}r = -pH_c$, whence $r_0 \ln (s/r_0)\,(\mathrm{d}r_0/\mathrm{d}t) = -p/\mu\sigma$. By integrating this expression with respect to time, and using the boundary condition $r_0 = s$ at $t = 0$, one obtains

$$1 - (r_0/s)^2\,\{1 - 2 \ln (r_0/s)\} = t/\tau, \tag{27}$$

where $\tau = \mu\sigma s^2/4p$ is the total time required for the destruction of the superconductivity.

When p is not very small compared to unity, i.e. when H_e is not very close to H_c, the field in the normal region may no longer be put equal to H_c. A

slightly more complicated expression for the total transition time then arises. Faber [53,3]) has found this expression to be

$$\tau = \frac{\mu\sigma s^2}{4} \frac{(1+p)}{p} . \tag{28}$$

The ratio of the volume fraction of normal material to the total volume of the specimen as a function of time is easily found on the basis of the eddy-current theory. This ratio is plotted against t/τ in figure 43. The curve in figure 43 is valid for all temperatures between zero and T_c.

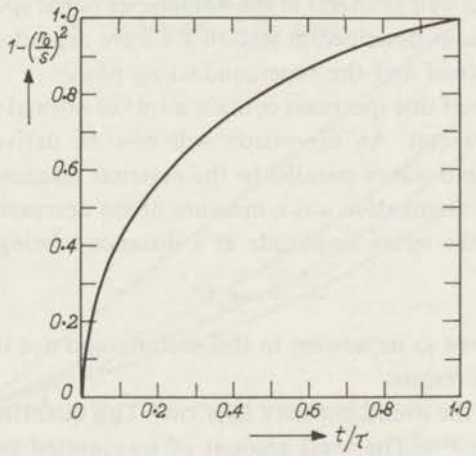

Fig. 43. Fraction of normally conducting material in a cylinder as a function of time after an external magnetic field parallel to the axis has been switched on divided by the total transition time, according to Pippard's eddy-current theory.

Measurements by Chopra and Hutchison [59,1]) of phase transition times in an aluminium specimen of diameter 20 mm, containing 60 p.p.m. of impurities, show qualitatively the field dependence suggested by equation (28). For thicker polycrystalline specimens the transition is rather irregular, which is ascribed by the authors to a movement of different domains at different rates.

The situation becomes more complicated when the intermediate state is established due to an external field smaller than H_c. Observations by means of powder photography on aluminium by Faber [58,4]) have indicated that for all values of H_e up to H_c, all normal regions are interconnected. Faber has suggested that the magnetic flux penetrates into the specimen through narrow slots at a rate which is approximately inversely proportional to the electrical conductivity. The interconnection of the normally conducting regions is asserted to be responsible for flux leakage at the transition from the normal to the superconducting phase [55,7]).

A formal description will now be given of ultrasonic absorption in an intermediate-state specimen at an external magnetic field H_e parallel to the propagation direction of the sound waves. This description will be used in section 4.2 for the interpretation of the experimental results on the kinetics of phase transitions. We assume the specimen to have plane-parallel end faces, and the sound waves to be propagated parallel to the axis of the specimen. The external magnetic field is thus also parallel to the axis of the specimen. We shall also assume the phase boundaries to be exactly parallel to the external magnetic field H_e and therefore parallel to the axis of the specimen. The transducer is supposed to have the same diameter as the specimen, and we neglect spreading of the sound beam as well as effects at the boundaries of the specimen. Furthermore, all the corrections described in section 2.4.2 are neglected, since they are the same for the normal and the superconducting phase.

Let a cross-section of this specimen contain a cm^2 of normal metal and b cm^2 of superconducting metal. An expression will now be derived for the total absorption α_k of sound waves parallel to the external magnetic field. We saw in chapter 1 that the attenuation α is a measure of the decrease in stress amplitude with distance, the stress amplitude at a distance x being given by

$$|\sigma| = \sigma_0 e^{-\alpha x}. \tag{1}$$

We note that α is given in nepers/cm in this section, and not in decibels/cm as for the experimental results.

We now introduce the sound intensity I per cm^2. This quantity is proportional to $|\sigma|^2$, and thus to $e^{-2\alpha x}$. The total amount of transmitted energy is proportional to $ae^{-2\alpha_n x} + be^{-2\alpha_s x}$. We now define the total absorption α_k by equating this sum with $(a + b)\, e^{-2\alpha_k x}$. Substituting $x = 1$ in this equation gives

$$\frac{a}{a+b}\, e^{-2\alpha_n} + \frac{b}{a+b}\, e^{-2\alpha_s} = e^{-2\alpha_k}, \tag{29}$$

whence

$$\alpha_k = -\tfrac{1}{2} \ln \frac{ae^{-2\alpha_n} + be^{-2\alpha_s}}{a+b} =$$

$$= \alpha_s - \tfrac{1}{2} \ln \frac{ae^{-2(\alpha_n - \alpha_s)} + b}{a+b} =$$

$$= \alpha_s - \tfrac{1}{2} \ln \left[e^{-2(\alpha_n - \alpha_s)} + \frac{b}{a+b} \{ -e^{-2(\alpha_n - \alpha_s)} + 1 \} \right].$$

Putting $e^{-2(\alpha_n - \alpha_s)} = \delta$, we have

$$\alpha_k = \alpha_s - \tfrac{1}{2} \ln \left\{ \delta + \frac{b}{a+b} (1 - \delta) \right\} =$$

$$= \alpha_s - \tfrac{1}{2} \ln \left(\frac{b}{a+b} + \delta \frac{a}{a+b} \right). \qquad (30)$$

The attenuation for the intermediate state, normalized with respect to $\alpha_n - \alpha_s$, is plotted in figure 44 as a function of the fraction of normally conducting material, for three values of δ, namely 0·05, 0·10 and 0·20.

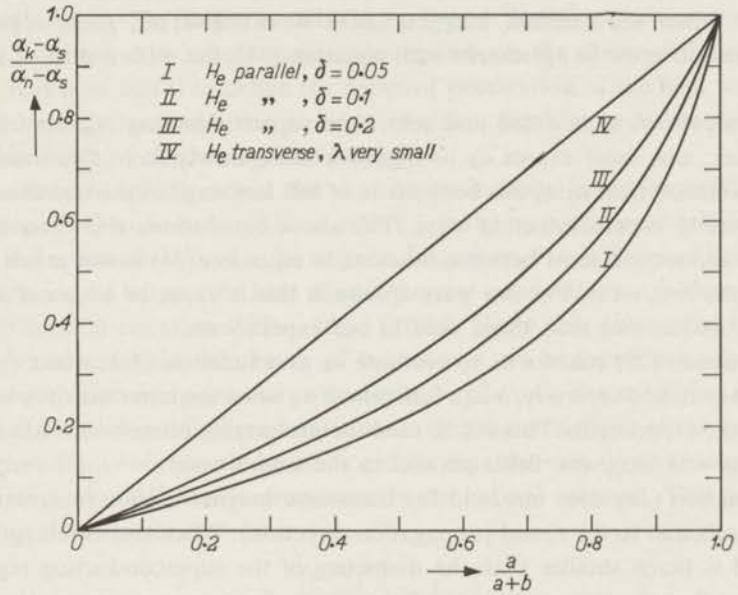

Fig. 44. Attenuation as a function of fraction of normally conducting material.

We shall suppose the specimen to be first in the normal state at $T < T_c$ at an external magnetic field $H_e \geqslant H_c$ parallel to the sound beam and we shall give a working model of what happens when this magnetic field is switched off suddenly. We assume that superconducting nuclei originate at different sites, and grow to filaments through the specimen parallel to the external magnetic field in a negligibly short time [50,1]). Those filaments grow transversely into the normal metal at a much lower rate. We assume further that the diameters of these superconducting regions increase proportionally to the time. Their volumes are proportional to the square of the diameters, and therefore proportional to the square of the time t, $t = 0$ being taken as the time when the filaments start to grow perpendicular to the magnetic field. We shall suppose $\alpha_s \ll \alpha_n$. This holds for high enough frequencies, when the temperature is not very close to T_c. In our experiments with magnetic fields parallel to the sound beam it was found that $\alpha_n - \alpha_s$ is of the order of 1 neper/cm. Therefore δ is substantially smaller than unity, and α_k can be written as a function of time:

$$\alpha_k - \alpha_s = c_1 - \log_e t - c_2\delta/t^2 + \ldots, \tag{31}$$

where c_1 and c_2 are time-independent factors.

A linear relation has therefore to be expected between the attenuation and the logarithm of time, except for very low values of t.

When the specimen is in the intermediate state under the influence of an external magnetic field H_e smaller than H_c, superconducting regions already exist. When the external magnetic field is switched off, these regions are assumed to grow in agreement with equation (31), but with a shift of the time scale.

This process is modified just before the superconducting regions touch one another; one must expect α_k to diminish more slowly from this time on. So far, no theoretical study has been made of this last stage of the transition to the completely superconducting state. The above conclusions also cease to apply when the second term between brackets in equation (31) is not much smaller than the first term. For our pure specimen this is expected to occur at much lower frequencies than those used in our experiments.

Equation (29) enables us to evaluate α_k as a function of b, when α_n and α_s are known, and inversely, b as a function of α_k when the latter quantity is known from the experiments. This will be used for interpreting phase-transition measurements with magnetic fields parallel to the sound beam.

Equation (29) does not hold for transverse magnetic fields (magnetic fields perpendicular to the sound-propagation direction). When the wavelength of the sound is much smaller than the diameters of the superconducting regions, it follows that the intermediate-state absorption for transverse magnetic fields is

$$\alpha_k = \frac{a}{a+b}\alpha_n + \frac{b}{a+b}\alpha_s, \tag{32}$$

whence

$$\alpha_k - \alpha_s = \frac{a}{a+b}(\alpha_n - \alpha_s). \tag{33}$$

This equation is represented by the straight line in figure 44. Equation (32) will become somewhat more complicated when the wavelength of the sound is of the same order of magnitude as the diameters of the superconducting regions, as happened in part of the measurements described in section 4.2.3. Although for this transition from the normal to the superconducting state the relation $b \propto t^2$ still holds, the relationship between the attenuation and the time is more complicated than for parallel magnetic fields, because of the frequency dependence.

All phase transitions are assumed to be isothermal. If phase transitions are adiabatic instead of isothermal, the transition from the superconducting to the

normal state may be expected to result in a local drop in temperature. The condition for the phase transitions to be isothermal was derived by Pippard [50,1]) on the basis of the following considerations. As mentioned above, Pippard assumes the superconducting region to be a single core of gradually decreasing radius. The depth of the phase boundary t seconds from the beginning of the transition from the superconducting state to the normal state, can be shown to be proportional to the skin depth for electromagnetic waves of circular frequency $\omega = t^{-1}$. The proportionality factor is $p\,(= H_e/H_c - 1)$ times a numerical factor of order unity whose magnitude depends on the shape of the specimen only. It is now useful to define the depth of penetration of the heat wave produced by the phase transition in terms of a skin depth in complete analogy to the skin depth of electromagnetic waves.

For electromagnetic waves the skin depth is easily found from Maxwell's equations [62,9]) to be $\delta_e = \sqrt{2/\mu\sigma\omega}$, where μ is the magnetic permeability, σ the electrical conductivity and ω the angular frequency. Propagation of heat waves through a solid of specific heat C and thermal conductivity κ is described by the differential equation $\nabla^2 T = (C/\kappa)\,(\partial T/\partial t)$. From this differential equation the expression for the skin depth of heat waves can be found in a way similar to that for electromagnetic waves to be $\delta_h = \sqrt{2\kappa/\omega C}$. The condition given by Pippard for isothermal phase transitions is that the skin depth of the heat wave at a given frequency should be much greater than the skin depth for an electromagnetic wave of the same frequency in the normal material. This condition leads to the expression

$$\left(\frac{\mu\sigma\kappa}{C}\right)^{1/2} \gg 1\,. \tag{34}$$

Taking typical values of σ, κ and C for pure normally conducting aluminium, we find $(\mu\sigma\kappa/C)^{\frac{1}{2}}$ to be between 10^2 and 10^3, so that condition (34) is satisfied. The temperature of a pure aluminium specimen will therefore be uniform during the phase transformation.

The question remains, whether the thermal contact between the liquid ^{3}He and the aluminium specimen is so good that no temperature difference arises. Fairbank and Lee [57,8]) have demonstrated the existence of a Kapitza resistance for ^{3}He. The value of this Kapitza resistance is of the order of $0{\cdot}013/T^2$ degrees m^2 watt $^{-1}$.

The energy difference between the normal phase and the superconducting phase for our aluminium specimen was estimated to be $2{\cdot}5\,.\,10^{-5}$ J at 1·05 °K, $10{\cdot}3\,.\,10^{-5}$ J at 0·90 °K and $28\,.\,10^{-5}$ J at 0·63 °K, assuming the volume of the specimen to be 10 cm^3. Supposing 4 cm^2 of the aluminium to be in direct contact with ^{3}He liquid, and furthermore supposing that the superconducting phase grows in proportion with time for one minute, the temperature rise of

the specimen at the transition from the normal to the superconducting phase was estimated for the three temperatures at which measurements have been performed. At 1·05 °K the increment is 0·012 millidegrees, at 0·90 °K 0·069 millidegrees and at 0·63 °K 0·39 millidegrees. Those increments may safely be neglected.

In these calculations the existence of the brass specimen holder was not taken into account. When the thermal contact between the aluminium and the specimen holder and the Kapitza resistance between the ^{3}He and the specimen holder are considered, the influence of the Kapitza resistance becomes even less than estimated above.

4.2. The experiments

4.2.1. *The experimental method*

The measurements described below were carried out on the zone-refined single crystal with orientation (100). The ultrasonic attenuation in the crystal was measured at regular intervals of 6 seconds after the switching on of the external magnetic field. Sometimes larger intervals were used, when the attenuation did not change rapidly. The experimental run was continued till the attenuation did not change appreciably. The field was then switched off and a second series of measurements made. The magnetic fields used for the experiments had values of between 0·6 and 1·4 H_c.

The experiments were performed in order to obtain information about the velocities at which phase boundaries are propagated during the transition from the superconducting state to the intermediate state and to the normal state and vice versa. It was also intended to study the structure of the intermediate state, especially the dimensions of the superconducting regions with respect to the wavelength of the sound. Sound waves of different wavelengths were therefore used, and measurements were performed with external magnetic fields both parallel and perpendicular to the sound-propagation direction. Information about the influence of the interphase surface energy on the structure of the intermediate state could be obtained by performing some of the measurements at three different temperatures, namely at 0·63, 0·90 and 1·05 °K.

The electronic equipment was the same as described in chapter 2. An *X*-cut quartz crystal with a main resonance frequency of 5 MHz was used for generating longitudinal sound waves, and a *Y*-cut crystal with the same main resonance frequency for generating shear waves.

A brass solenoid was used for producing the magnetic fields parallel to the sound-propagation direction, and a Helmholtz coil for producing the fields perpendicular to this direction. Both magnets were carefully calibrated with a Rawson rotating-coil gauss meter, type 7298. The solenoid had previously been calibrated by measuring critical fields in an indium specimen at different tem-

peratures between 1 °K and T_c [54,3]). For that solenoid the results of the two calibrations and of the theoretical calculations were in excellent agreement with one another. The calibration constants were 42 Oe/A for the solenoid and 43 Oe/A for the Helmholtz coil. A d.c. voltage of 24 V was applied to the magnets, variable resistors being used to adjust the magnetic fields to the desired values.

A clockwork-operated bell produced a signal every six or twelve seconds. Each time the bell rang the ultrasonic attenuation was measured by adjusting the height of the standard signal to that of one of the peaks on the screen of the oscilloscope by means of a Rohde & Schwarz unbalanced standard attenuator. That part of the attenuation which was independent of the temperature and of the magnetic field was eliminated by performing a series of measurements of attenuation as a function of the temperature at zero external field. The procedure for eliminating that part of the attenuation has been explained in section 3.1.3.

4.2.2. *Phase transitions with parallel external fields*

TABLE V

Phase-transition measurements with parallel external fields

serial number	temperature (°K)	sound waves	frequency (MHz)	H_e parallel (Oe)
7	0·90	transv.	15·1	50½
8	0·63	transv.	15·1	87½
9	1·05	transv.	15·1	24½
16	0·63	long.	26·0	87½

Table V shows a number of sets of measurements that were performed with external magnetic fields H_e parallel to the sound-propagation direction. The ultrasonic attenuation was measured as a function of time in order to study phase transitions from the superconducting state to the intermediate state and to the normal state and vice versa. The values of the critical fields were obtained from the measurements described in section 3.3. Corrections have to be made for the values of these critical fields as well as for the other parallel external fields H_e of this section, because of the influence of the superconducting solder, mentioned at the end of chapter 3. The measured field strengths have to be multiplied by about 0·86 in order to obtain the effective field strengths. This correction, however, does not influence the value of $p = (H_e - H_c)/H_c$ very strongly.

Figure 45 shows the results of the measurements with longitudinal sound waves of 26·0 MHz, for studying phase transitions from the superconducting state to the intermediate state and to the normal state, at 0·63 °K (series 16).

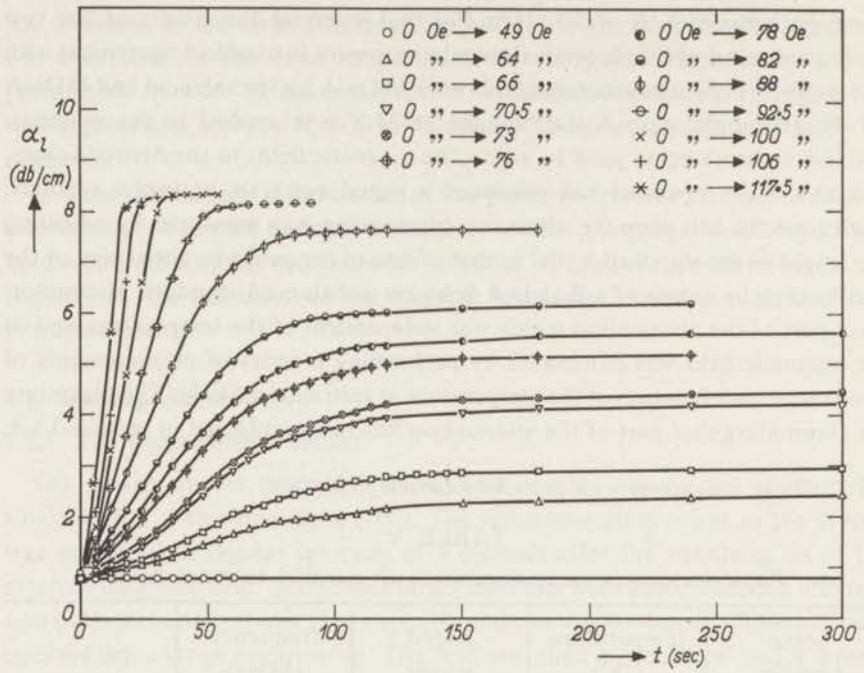

Fig. 45. Absorption of 26·0-MHz longitudinal sound waves at 0·63 °K as a function of time after parallel magnetic fields have been switched on.

Similar sets of measurements were performed with 15·1-MHz shear waves, at three different temperatures, 0·63, 0·90 and 1·05 °K. The results of these measurements are similar to those when longitudinal sound waves of 26·0 MHz are used; there is no evidence that the shape of the attenuation-time curve at a fixed value of H_e/H_c depends on the kind of sound waves or on the temperature. The results will now be discussed.

(*a*). $H_e = 0 \rightarrow H_e > H_c$

The measurements on transitions from the superconducting state to the normal state show that the time needed for obtaining normal-state attenuation decreases with increasing magnetic field. This is in qualitative agreement with the eddy-current theory by Pippard. A quantitative analysis of the results requires a definition of the phase-transition time τ. This time τ is defined as the interval between zero time and the moment when the attenuation attains a constant value; see figure 45. It is assumed that the whole transition from the superconducting to the normal state takes place during this interval. According to equation (28) given by Faber the time τ should be proportional to $(1 + p)/p$, where p is defined by $H_e = H_c\,(1 + p)$. In order to check this relation the transition time τ was determined for all experimental runs belonging to series 7, 8, 9 and 16, where the external fields exceeded the critical field. These values of τ

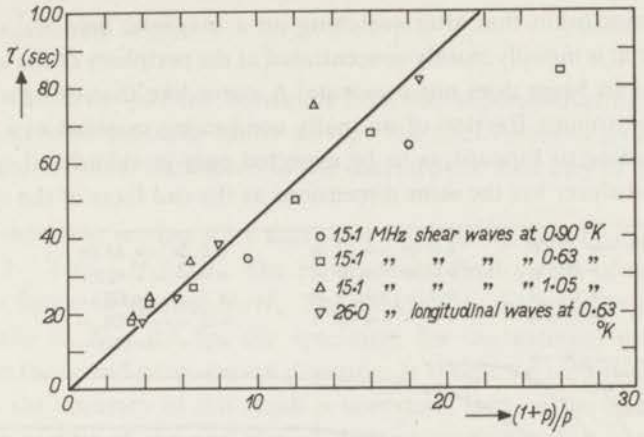

Fig. 46. Total time of transition from the superconducting state to the normal state as a function of $(1 + p)/p$ with parallel magnetic fields.

are plotted against $(1 + p)/p$ in figure 46, which gives some evidence for a linear relation between τ and $(1 + p)/p$. The slope of this graph is apparently not dependent on the temperature.

There is some scattering in the measured values plotted in figure 46. The first reason for this scattering is the inaccuracy of determining the transition times from the measurements. The second reason is the inaccuracy in determining the values of the critical fields. This causes deviations from the linear relation for fields very near the critical field, where $(1 + p)/p$ is very large. It should also be mentioned that the description given by Pippard and Faber based upon the eddy-current theory is asserted to hold for cylindrical specimens, whereas the specimen used in the actual experiments was not completely cylindrical. Still, equation (28) may be expected to hold to a good approximation for our specimen.

Using equation (28), the resistivity of the specimen was estimated from figure 46. The slope of the graph is 4·6 sec. Assuming the area of an end face of the specimen to be 3 cm^2, we found the electrical conductivity σ to be $1{\cdot}5 \cdot 10^{11}\ \Omega^{-1}m^{-1}$, so that the specific resistivity is equal to $7 \cdot 10^{-12}\ \Omega m$. As the specific resistivity of the specimen was not determined at liquid-helium temperatures, it is impossible to check this result, but it is certainly of the right order of magnitude.

The volume fraction of normal material $a/(a + b)$ in the sound beam was now calculated from the attenuation values by using equation (29). This led to one value of $a/(a + b)$ for each measured value of the attenuation α_k. The values of $a/(a + b)$ thus determined are plotted in figure 47 as a function of time for the 26·0-MHz longitudinal sound waves at 0·63 °K.

Each curve in figure 47 starts rising much more slowly than predicted by the eddy-current theory. This is not surprising, as the diameter of the transducer is smaller than the dimensions of the end faces of the specimen. These results

lead to the conclusion that after switching on a magnetic field $H_e > H_c$, the normal material is initially mainly concentrated at the periphery of the specimen, where the sound beam does not penetrate. A curve like that of figure 43, representing the volume fraction of normally conducting material as a function of time according to Pippard, is to be expected only in cylindrical specimens where the transducer has the same dimensions as the end faces of the specimen.

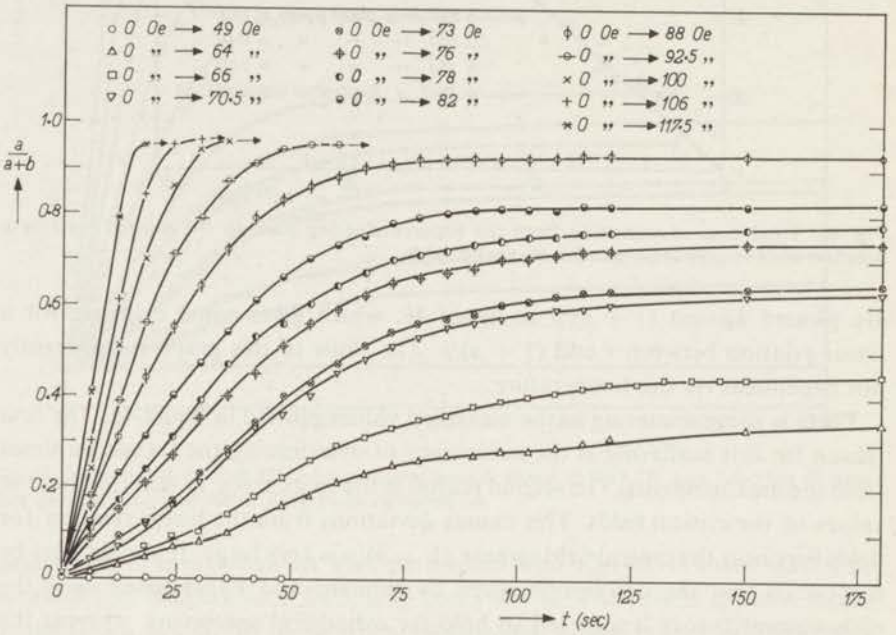

Fig. 47. Fraction of normally conducting material in the sound beam as a function of time for the measurements of figure 44.

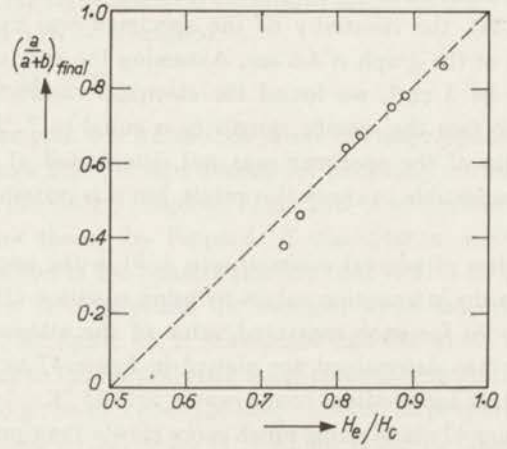

Fig. 48. Final fraction of normally-conducting material in the sound beam for the intermediate state as a function of external field divided by critical field for the measurements of figure 44, at $H_e < H_c$.

(*b*). $H_e = 0 \rightarrow H_e < H_c$

Figure 45 shows that the transition from the superconducting state to the intermediate state proceeds rather slowly. The final values of $a/(a + b)$ in the sound beam for these transitions to the intermediate state can be read off from figure 47.

It was shown in section 4.1.1 that these final values may be expected to be equal to $1 - (H_c - H_e)/DH_c$. The experimental final values of $a/(a + b)$ are plotted in figure 48 against H_e/H_c. The broken line through the experimental points leads to $D = 0{\cdot}5$ for the specimen, for the external magnetic field parallel to the sound-propagation direction. It should be remarked here, however, that the accuracy of this result is uncertain, because the transducer only covers the middle of the end face of the specimen. Another reason why the value of D is not accurate is that the solder used for the ^{3}He cryostat was superconducting during the experiments. This should lead to an additional deformation of the lines of force around the specimen.

(*c*). $H_e > H_c \rightarrow H_e = 0$ *and* $H_e < H_c \rightarrow H_e = 0$

Figure 49 shows the results of the measurements with longitudinal sound waves of 26·0 MHz, for studying phase transitions from the normal state and from the intermediate state to the superconducting state at 0·63 °K (series 16). Similar results were obtained for series 7, 8 and 9. There is again no evidence that the shape of an attenuation-time curve at a fixed value of H_e/H_c depends

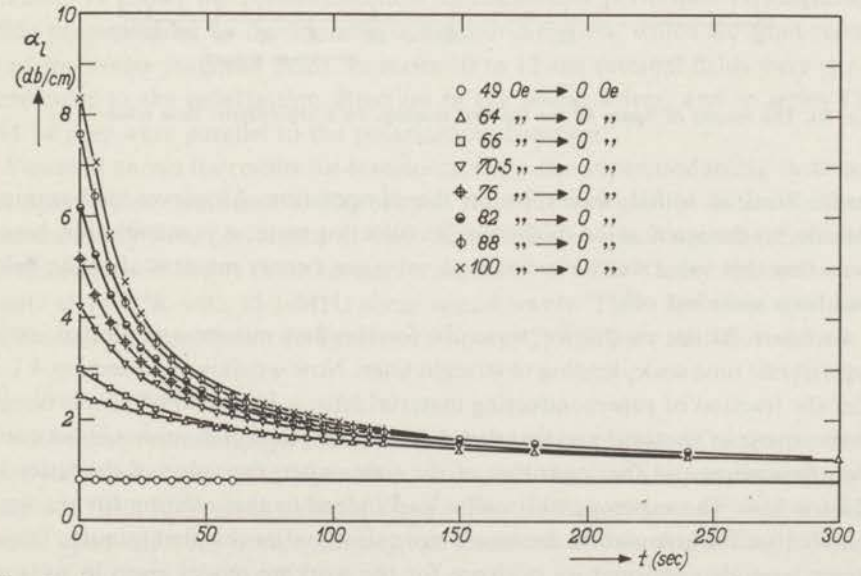

Fig. 49. Absorption of 26·0-MHz longitudinal sound waves at 0·63 °K as a function of time after parallel magnetic fields have been switched off.

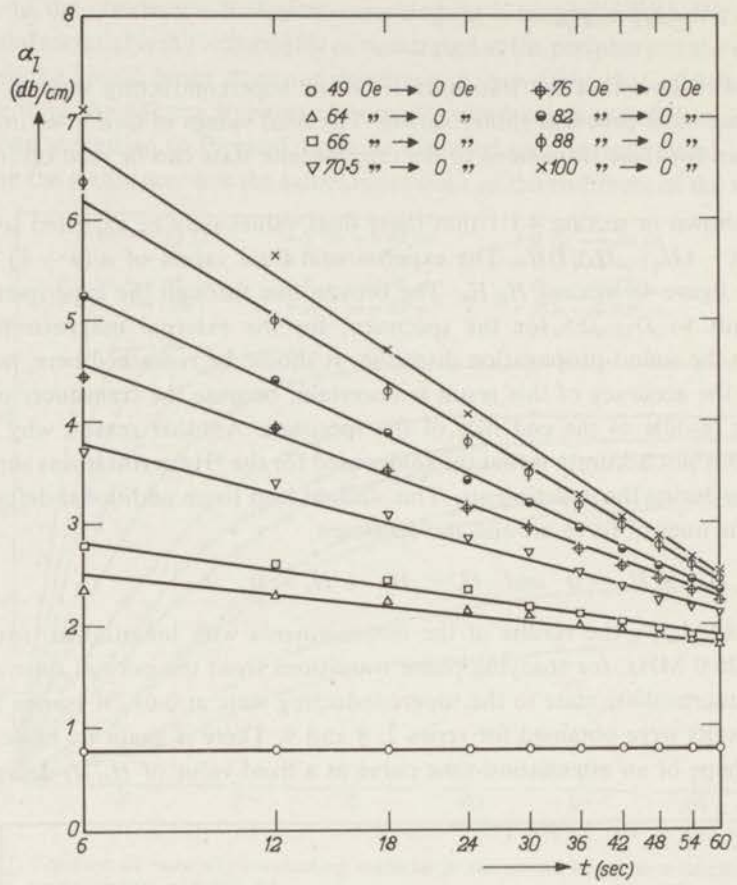

Fig. 50. The results of figure 48 for the first minute, on a logarithmic time scale.

on the kind of sound waves or on the temperature. All curves tend asymptotically to the attenuation of the superconducting state; it is remarkable, however, that this value was never reached, even not twenty minutes after the field had been switched off.

In figure 50 the results for series 16 for the first minute are plotted on a logarithmic time scale, leading to straight lines. Now we showed in section 4.1.3 that the fraction of superconducting material $b/(a + b)$ should be proportional to the square of the time, and that therefore a linear relation should exist between the attenuation and the logarithm of the time, when the value of the latter is not too low. The experimental results lead indeed to this relation for the first minute, but the attenuation decreases more slowly after this first minute. These results provide confirmatory evidence for the working model given in section 4.1.3. In order to obtain a more accurate analysis of those phase transitions it

would seem to be necessary to perform experiments where the sound beam covers the whole specimen.

4.2.3. *Phase transitions with transverse external fields*

TABLE VI

Phase-transition measurements with transverse external fields

serial number	temperature (°K)	sound waves	orientation H_e	frequency (MHz)	H_c parallel (Oe)	H_c transverse (Oe)
10	0·90	transv. {010}	{001}	15·1	50½	43½
11	0·63	transv. {010}	{001}	15·1	87½	75
12	1·05	transv. {010}	{001}	15·1	24½	20½
13	0·63	transv. {010}	{010}	15·1	87½	75
14	0·63	transv. {010}	{010}	5	87½	75
15	0·63	long. {100}	{010}	26·0	87½	75
17*)	0·63	long. {100}	{010}	15·2	87½	75

Table VI shows the phase-transition measurements performed at magnetic fields perpendicular to the sound-propagation direction, which we shall refer to as transverse magnetic fields. In series 10 to 12 the external fields were perpendicular to the polarization direction of the sound waves, and in series 13 and 14 they were parallel to the polarization direction.

Figure 51 shows the results for transitions from the superconducting state to the intermediate state and to the normal state for series 15 of table VI. The measurements were performed at 0·63 °K with 26·0-MHz longitudinal sound waves. Figure 52 shows those results for series 12 of table VI, for the measurements at 1·05 °K with 15·1-MHz shear sound waves. There are some obvious differences between those two figures and figure 45, which we shall now discuss.

(*a*). $H_e = 0 \rightarrow H_e > H_c$

Each curve representing a transition from the superconducting to the normal state starts much more steeply with a transverse than with a parallel external magnetic field, for a given value of H_e/H_c. This is in agreement with the model based upon the eddy-current theory, as discussed above. According to that

*) For series 17 no measurements of transitions from the superconducting to the normal state and vice versa were performed.

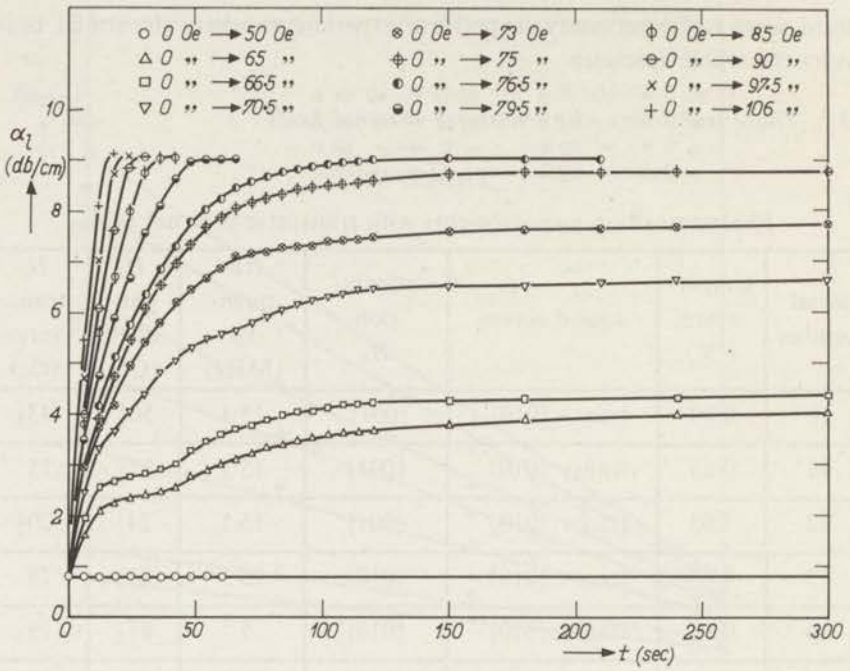

Fig. 51. Absorption of 26·0-MHz longitudinal sound waves at 0·63 °K as a function of time after transverse magnetic fields have been switched on.

model it is to be expected that initially, after switching on an external magnetic field $H_e > H_c$, a great deal of the normal material is concentrated near the boundaries running parallel to the external magnetic field. Therefore with transverse external fields a substantial part of the normal material is initially found near the end faces of the specimen, and contributes to the attenuation, whereas for parallel external fields the greater part of the normal material is initially found in that part of the specimen that is not covered by the sound beam. The difference in measured critical fields for parallel and for transverse external fields has already been explained as being caused by the superconducting solder used for the ^{3}He cryostat. The values of the critical fields measured with transverse external fields proved to be in excellent agreement with the critical-field measurements by Goodman and Mendoza.

For the measurements with transverse external magnetic fields the times of transition from the superconducting phase to the normal phase were again defined as the interval between zero time and the moment when the attenuation attains a constant value. These transition times were determined for series 10 to 15, and were compared with each other for the same values of H_e/H_c. It was shown in section 4.2.2 that with parallel external fields there was no evidence that the transition times depend on the temperature. This is not true with transverse external fields. The transition times proved to be shortest at the lowest

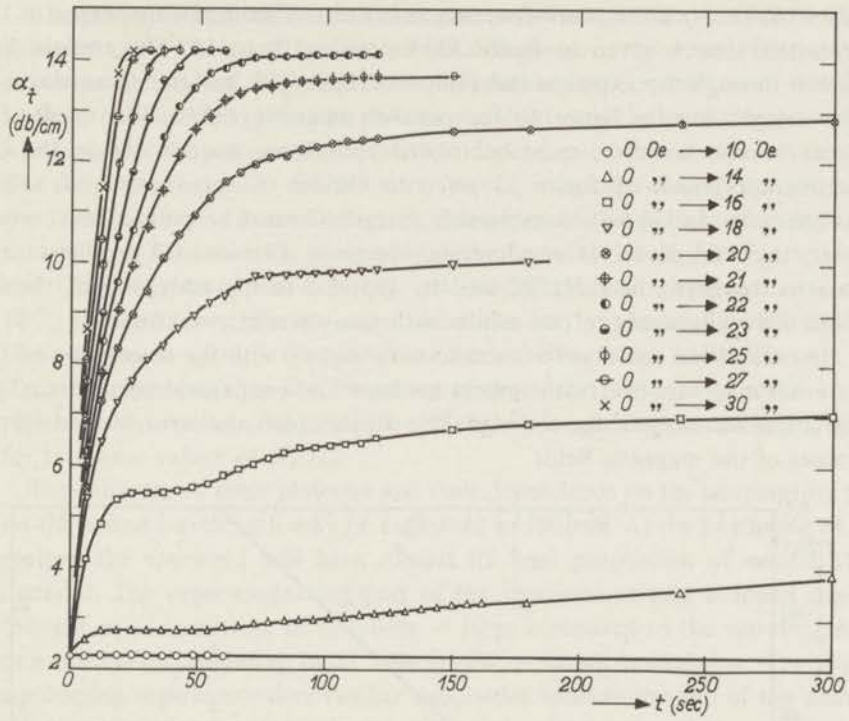

Fig. 52. Absorption of 15·1-MHz shear sound waves at 1·05 °K as a function of time after transverse magnetic fields have been switched on.

temperatures, at comparable values of H_e/H_c. The transition times at 0·90 °K and at 1·05 °K were about 25% longer than those for 0·63 °K, for the same ratios of H_e/H_c. Comparison of the results of series 13 and 14 did not show any evidence that the transition times depend on the sound wavelength.

The temperature dependence of the transition times can be ascribed qualitatively to the temperature dependence of the interphase surface energy. At 0·63 °K this energy is lower than at the higher temperatures. This causes a closer spacing of the superconducting regions in the intermediate state for 0·63 °K, and therefore smaller superconducting regions, i.e. a larger ratio of the wavelength to the dimensions of the superconducting regions. One may expect that the transition times would be found to depend on the wavelength of the sound, if a larger frequency range were covered.

In the model for the intermediate state as described above, scattering of the sound waves at the interphase boundaries has not been taken into account. This scattering was estimated to be negligibly small compared to the total attenuation, which is not surprising as it is a second-order effect.

The time of transition from the superconducting phase to the normal phase has been determined as a function of p', where p' is defined by

$H_e = H_c(1 + p')$ for transverse magnetic fields. This field dependence of the transition time is given in figure 53, for series 10 to 15. The straight line drawn through the experimental points of figure 53 has the same slope as the straight line in figure 46 for parallel magnetic fields. The results for shear waves, however, must be treated with some caution, since the experimental points of figure 53 refer to various temperatures and sound wavelengths, and show a considerable spread. It must be pointed out, moreover, that the model of a cylindrical specimen with its axis parallel to the external magnetic field H_e, as used by Pippard in his eddy-current theory, does not really apply to our results with transverse external fields.

The transition times were found to vary slightly with the orientation of the external magnetic field with respect to the sound-propagation direction. This variation was only of the order of 2%, which equals the error in reading the values of the magnetic fields.

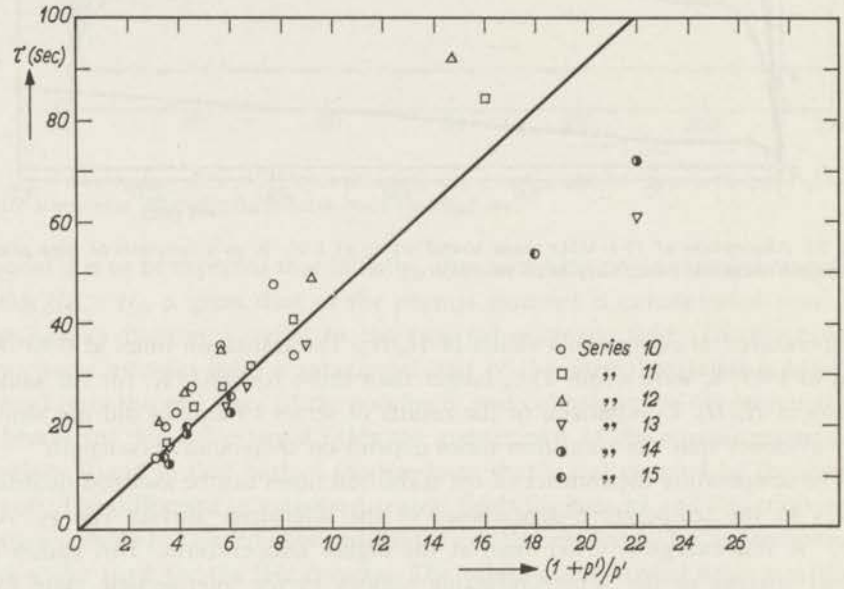

Fig. 53. Total time of transition from the superconducting state to the normal state as a function of $(1 + p')/p'$; p' is defined with reference to the transverse external fields.

(*b*). $H_e = 0 \rightarrow H_e < H_c$

The curves representing the attenuation as a function of time after switching on an external magnetic field are different in shape for parallel external fields and for transverse external fields, especially for the transitions $H_e = 0 \rightarrow H_e < 0{\cdot}9\, H_c$. This is evident when figures 45 and 51 are compared with each other. With transverse external fields there is an almost flat "plateau" between 10 and 50 sec for the lowest fields.

The plateau was found at transverse external fields smaller than 0·9 H_c for all series 10 to 15. There are, however, small differences in the shape of the plateau at comparable values of H_e/H_c for the different series. Comparison of series 10, 11 and 12 shows clearly that the plateau was shortest at the lowest temperatures. The length of the plateau also appears to depend somewhat on the wavelength. For series 14, that is for 5-MHz shear waves, it is somewhat shorter than for the 15-MHz shear waves of series 13. For series 15 this plateau has about the same size as for series 13, always for the same values of H_e/H_c. For series 13 and 15 the frequency was different, but the difference in wavelength was only 10%, owing to the different sound velocities for longitudinal waves and for shear waves. It appears therefore that the wavelength has more effect on the size of the plateau than the frequency of the sound waves. For series 17 the plateau is shorter than for series 15, and slightly longer than for series 14, again for the same values of H_e/H_c.

The existence of these plateaux and their dependence on the temperature and on the sound wavelength may be explained as follows. At the beginning of the plateau the specimen will have almost its final proportion of normal-state material. The superconducting part of the specimen at that moment can be thought of as consisting of cylinders — large compared to the wavelength — in a normally conducting bulk. This is still an unstable situation. The superconducting regions are then further subdivided until at the end of the plateau the diameter of the superconducting regions is of the order of the sound wavelength. When the superconducting regions are further split up into smaller cylinders, so that their diameters become smaller than the sound wavelength, they will cause a higher value of the sound attenuation. For external magnetic fields parallel to the sound-propagation direction, on the other hand, the attenuation is only dependent on the fraction of superconducting metal, and not on the dimensions of the superconducting regions.

The foregoing also explains why at the largest sound wavelength, i.e. at the lowest frequency, for a given kind of sound waves, the attenuation starts to rise from the plateau more rapidly than at smaller wavelengths. Differences at different temperatures must again be attributed to differences in interphase surface energy. This energy decreases with decreasing temperature, and therefore at 0·63 °K the superconducting cylinders have smaller diameters than at higher temperatures. This means that the situation where the sound wavelength exceeds these diameters, and α_k increases accordingly, occurs more rapidly at 0·63 °K than at the higher temperatures, giving rise to a shorter plateau.

(*c*). $H_e > H_c \rightarrow H_e = 0$ *and* $H_e < H_c \rightarrow H_e = 0$

Figure 54 shows the results for transitions from the normal state and from the intermediate state to the superconducting state, again for series 15. The striking difference between these results and those of the measurements with

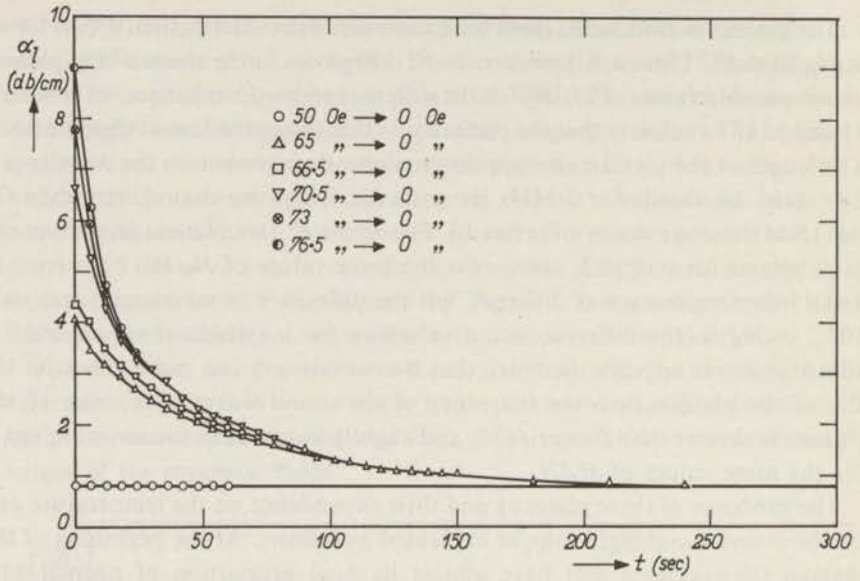

Fig. 54. Absorption of 26·0-MHz longitudinal sound waves at 0·63 °K as a function of time after transverse magnetic fields have been switched off.

parallel external fields is that here the attenuation value for the superconducting state is already attained about four minutes after switching the magnetic field off. No evidence could be found for a dependence of this time on the temperature or on the frequency, as no essential difference appeared between the results of each of the series 10 to 15.

The measurements at transverse external magnetic fields lead to the conclusion that within four minutes after switching off the magnetic field only normal regions remain whose dimensions perpendicular to the sound-propagation direction are much smaller than the wavelength of the sound. These normal regions are assumed to be undetected by the sound waves, so that the attenuation will correspond to the superconducting state, even though a part of the specimen is still normally conducting. With parallel external magnetic fields, on the other hand, the attenuation remains dependent on the fraction of normal material, and independent of the dimensions of the normal regions. The attenuation will only be equal to α_s when no normal fraction is left. Our measurements with parallel external fields indicate that the normal fraction continues to exist for much longer than four minutes, since the attenuation did not attain the value for the superconducting state even after twenty minutes.

4.2.4. *Measurements on less pure aluminium*

The considerations of section 4.1 suggest that it would be interesting to perform ultrasonic measurements during phase transitions in aluminium specimens with different amounts of impurities. One could determine the transition times

from the superconducting state to the normal state as a function of the impurity of the specimen, and measurements in a larger frequency range similar to the measurements described in sections 4.2.2 and 4.2.3 would lead to knowledge of the dimensions of the superconducting regions and their spacing when the specimen is in the intermediate state.

We have found all transition times for specimens containing about 50 p.p.m. and 100 p.p.m. of impurities to be much shorter than the transition times for the zone-refined aluminium specimen. They were even so short that it was impossible to perform accurate ultrasonic measurements during the phase transitions with the experimental method described in section 4.2.1. Another experimental arrangement is therefore under construction for performing ultrasonic measurements during phase transitions lasting between 10 sec and 100 100 msec.

REFERENCES

50,1) Pippard, A. B., Phil. Mag. **XLI**, 243, 1950.
51,1) Goodman, B. B. and Mendoza, E., Phil. Mag. **XLII**, 594, 1951.
52,1) Faber, T. E., Proc. Roy. Soc. London A **214**, 392, 1952.
53,1) Tiller, W. A., Rutter, J. W., Jackson, K. and Chalmers, B., Acta Metall. **1**, 428, 1953.
53,2) Squire, C. F., Low temperature physics, McGraw-Hill, London, 1953, Chap. II.
53,3) Faber, T. E., Proc. Roy. Soc. London A **219**, 75, 1953.
54,1) Bömmel, H. E., Phys. Rev. **96**, 220 L, 1954.
54,2) Faber, T.E., Proc. Roy. Soc. London A **223**, 174, 1954.
54,3) Maxwell, E. and Lutes, O. S., Phys. Rev. **95**, 333, 1954.
55,1) Pippard, A. B., Phil. Mag. **46**, 1104, 1955.
55,2) Kittel, C., Acta Metall. **3**, 295, 1955.
55,3) Schiff, L. I. ,Quantum mechanics, McGraw-Hill, New York, 1955, 2nd edition, sec. 29.
55,4) Montariol, F., Thesis, Paris, 1955, Chap. III.
55,5) Caron, M., Thesis, Paris, 1955.
55,6) Daunt, J. G., The electronic specific heat in metals, table 2, Progress in low temperature physics, Ed. C. J. Gorter, North-Holland Publ. Comp., Amsterdam, 1955, Vol. I, Chap. XI.
55,7) Faber, T. E. and Pippard, A. B., Kinetics of the phase transition in superconductors, Progress in low temperature physics, Ed. C. J. Gorter, North-Holland Publ. Comp., Amsterdam, 1955, Vol. I, Chap. IX.
55,8) Faber, T. E., Proc. Roy. Soc. London A **231**, 353, 1955.
56,1) Mason, W. P. and Bömmel, H. E., J. acoust. Soc. Amer. **28**, 930, 1956.
56,2) Klemens, P. G., Thermal conductivity of solids at low temperatures, Encyclopaedia of physics, Ed. S. Flügge, Springer-Verlag, 1956, Vol. XIV.
56,3) Cullity, B. D., Elements of X-ray diffraction, Addison-Wesley, Reading, Mass., 1956, Chaps 2, 3 and 8.
56,4) Roberts, T. R. and Sydoriak, S. G., Phys. Rev. **102**, 304, 1956.
56,5) Seki, H., Granato, A. and Truell, R., J. acoust. Soc. Amer. **28**, 230, 1956.
56,6) Redwood, M. and Lamb, J., Proc. Inst. electr. Engrs **103**, Part B, 773, 1956.
56,7) Buckingham, M. J., Phys. Rev. **101**, 1431 L, 1956.
56,8) Schawlow, A. L., Phys. Rev. **101**, 573, 1956.
56,9) Cochran, J. F., Mapother, D. E. and Mould, R. E., Phys. Rev. **103**, 1657, 1956.
57,1) Bardeen, J., Cooper, L. M. and Schrieffer, J. R., Phys. Rev. **108**, 1175, 1957.
57,2) Glover, R. E. and Tinkham, M., Phys. Rev. **108**, 243, 1957.
57,3) Morse, R. W. and Bohm, H. V., Phys. Rev. **108**, 1094 L, 1957.
57,4) Nicol, J. and Soller, T., Bull. Amer. phys. Soc., Ser. II, Vol. **2**, 63, 1957.
57,5) Sydoriak, S. G. and Roberts, T. R., Phys. Rev. **106**, 175, 1957.
57,6) Balashova, B. M. and Sharvin, Iu. V., Soviet Phys. JETP, New York, **4**, 54, 1957.
57,7) Faber, T. E., Proc. Roy. Soc. London A **241**, 531, 1957.
57,8) Fairbank, H. A. and Lee, D. M., Proceedings of the 5th international conference on low temperature physics and chemistry, Wisconsin, The University of Wisconsin Press, Madison, 1957, p. 93.
58,1) Chopra, K. L. and Hutchison, T. S., Canad. J. Phys. **36**, 805, 1958.
58,2) Morse, R. W., J. acoust. Soc. Amer. **30**, 380, 1958.
58,3) Pfann, W. G., Zone melting, John Wiley and Sons, New York, 1958, Chaps 2 and 3.
58,4) Faber, T. E., Proc. Roy. Soc. London A **248**, 460, 1958.
58,5) Cochran, J. F. and Mapother, D. E., Phys. Rev. **111**, 132, 1958.
59,1) Chopra, K. L. and Hutchison, T. S., Canad. J. Phys. **37**, 614, 1959.
59,2) Morse, R. W. and Bohm, H. V., J. acoust. Soc. Amer. **31**, 1523, 1959.
59,3) Morse, R. W., Ultrasonic attenuation in metals at low temperatures, Progress in cryogenics, Ed. K. Mendelssohn, Heywood, London, 1959, Vol. I.
59,4) Biondi, M. A. and Garfunkel, M. P., Phys. Rev. **116**, 853, 1959.
59,5) Morse, R. W., Olsen, T. and Gavenda, J. D., Phys. Rev. Letters **3**, 15, 1959; erratum Phys. Rev. Letters **4**, 193, 1959.
59,6) Van Iersel, A. M. R., Thesis, Leiden, 1959, Chap. III.
60,1) Ziman, J. M., Electrons and phonons, Clarendon Press, Oxford, 1960, Chap. II.
60,2) Pippard, A. B., Reports on progress in physics **XXIII**, 176, 1960.
60,3) Ziman, J. M., Electrons and phonons, Clarendon Press, Oxford, 1960, Chap. V.
60,4) Cooper, L. N., Amer. J. Phys. **28**, 91, 1960.

60,5) Landau, L. D. and Lifshitz, E. M., Electrodynamics of continuous media, Pergamon Press, 1960, Sec. 44.
61,1) Bardeen, J. and Schrieffer, J. R., Recent developments in superconductivity, Progress in low temperature physics, Ed. C. J. Gorter, North-Holland Publ. Comp., Amsterdam, 1961, Vol. III, Chap. VI.
61,2) Bezuglyi, P. A., Galkin, A. A. and Korolyuk, A. P., Soviet Physics JETP, New York, **12**, 4, 1961.
61,3) Tsuneto, T., Phys. Rev. **121**, 402, 1961.
61,4) Taconis, K. W., ^{3}He cryostats, Progress in low temperature physics, Ed. C. J. Gorter, North-Holland Publ. Comp., Amsterdam, 1961, Vol. III, Chap. V.
61,5) Pokrovskii, V. L., Soviet Physics JETP, New York, **13**, 628, 1961.
62,1) Morse, R. W., IBM Journal **6**, 58, 1962.
62,2) Truell, R. and Elbaum, Ch., High frequency ultrasonic stress waves in solids, Encyclopaedia of physics, Ed. S. Flügge, Springer-Verlag, 1962, Vol. XI/2.
62,3) Kamm, G. N. and Bohm, H. V., Rev. scientific Instr. **33**, 957, 1962.
62,4) Barone, A., Generation, detection and measurement of ultrasound, Encyclopaedia of physics, Ed. S. Flügge, Springer-Verlag, 1962, Vol. XI/1, Sec. 15.
62,5) David, R., Van der Laan, H. R. and Poulis, N. J., Commun. Kamerlingh Onnes Lab., Leiden No. 331 c; Physica **28**, 330, 1962.
62,6) Masuda, Y. and Redfield, A. G., Phys. Rev. **125**, 159, 1962.
62,7) Levy, M., Kagiwada, R. and Rudnick, I., Proceedings of the 8th international congress on low temperature physics, Butterworth, London, 1962, p. 188.
62,8) Lynton, E. A., Superconductivity, Methuen, London, 1962, Chap. VI.
62,9) Panofsky, W. K. H. and Phillips, M., Classical electricity and magnetism, Addison-Wesley, Cambridge, Mass., 1962, 2nd edition, Chap. 11.
63,1) Blitz, J., Fundamentals of ultrasonics, Butterworth, London, 1963, Chap. 2.
63,2) Kamm, G. N., and Bohm H. V., Phys. Rev. **131**, 111, 1963.
63,3) Olsen, T., J. Phys. Chem. Solids **24**, 649, 1963.
63,4) David, R., Van der Laan, H. R. and Poulis, N. J., Commun. Kamerlingh Onnes Lab., Leiden No. 335a; Physica **29**, 357, 1963.
63,5) Olsen, T., J. Phys. Chem. Solids **24**, 187, 1963.
63,6) Levy, M., Phys. Rev. **131**, 1497, 1963.

SAMENVATTING

In dit proefschrift wordt de absorptie van ultrageluid in supergeleidend aluminium behandeld. De resultaten van de metingen met longitudinale geluidsgolven zijn voor preparaten van verschillende zuiverheid in overeenstemming met de theorie van Bardeen, Cooper en Schrieffer. Uit extrapolatie volgt dat de energiespleet bij temperatuur nul $3{\cdot}5\ kT_c$ is.

De absorptie van transversale geluidsgolven kan worden gesplitst in twee gedeelten, nl. één gedeelte dat aan de BCS-theorie voldoet, en één gedeelte, dat onder het sprongpunt voor de supergeleiding zeer snel afneemt, en bij 0·02 °K onder het sprongpunt verdwenen is. Dit tweede gedeelte van de absorptie is tevens verwaarloosbaar klein wanneer het produkt van golfgetal van het geluid en gemiddelde vrije weglengte van de elektronen veel kleiner is dan één. Dit wordt aangetoond met metingen bij een aantal frekwenties aan preparaten van verschillende zuiverheid. In twee eenkristallen van zonegesmolten aluminium zijn metingen uitgevoerd bij verschillende polarisatierichtingen van het geluid. De grootte van de absorptie hangt wel enigszins van de polarisatierichting af, de energiespleet echter niet.

Met behulp van ultrageluid zijn in een eenkristal van zeer zuiver zonegesmolten aluminium faseovergangen bestudeerd. Het doel van de experimenten was konklusies te trekken uit de snelheid waarmee de fasegrenzen zich voortplanten, en gegevens te krijgen over de struktuur van de tussentoestand. In verband met dit laatste zijn er metingen uitgevoerd bij verschillende temperaturen en bij verschillende frekwenties. De resultaten van de metingen zowel bij magneetvelden evenwijdig aan de voortplantingsrichting van het geluid als loodrecht er op zijn in overeenstemming met de theorieën van Pippard en Faber. Het verloop van de absorptie bij de overgang van de supergeleidende naar de normale fase bevestigt de beschrijving van Pippard die gebaseerd is op de kringstroomtheorie. Voor de overgang van de normale naar de supergeleidende fase kan een formele beschrijving worden gegeven, die eveneens voldoet. Er is gebleken, dat er in het zeer zuivere preparaat na het afzetten van een magneetveld van de orde van grootte van het kritische veld, langer dan twintig minuten dunne normaal-geleidende gebiedjes blijven bestaan. Alle overgangstijden zijn in minder zuiver aluminium aanmerkelijk korter dan in het zonegesmolten aluminium eenkristal.

INSTITUUT-LORENTZ
voor theoretische natuurkunde
Nieuwsteeg 18-Leiden-Nederland

STELLINGEN

I

In de grafiek van de absorptie van longitudinale geluidsgolven in supergeleiders tegen de temperatuur kan een afwijking van de theoretische kromme van Bardeen, Cooper en Schrieffer optreden ten gevolge van het feit, dat de „weak-coupling limit" geen juiste benadering meer is. Dit kan experimenteel worden geverifieerd.

R. Weber, Phys. Rev. **133**, A 1487, 1964.

II

De uitspraak van Claiborne en Einspruch, dat slingeringen in de kromme, die de absorptie van geluidsgolven in supergeleiders tegen de temperatuur weergeeft, als eigenschap van de supergeleidende toestand beschouwd moeten worden, is voorbarig.

L. T. Claiborne en N. G. Einspruch, Phys. Letters **8**, 160, 1964.

III

De Debije-Hueckel-lengte speelt bij de wisselwerking tussen ultrageluid en ladingdragers in piëzo-electrische halfgeleiders een andere rol dan in niet-piëzo-electrische stoffen.

IV

De wijze waarop Barua en Saran tot een temperatuurafhankelijkheid van de polariseerbaarheid van waterstof en deuterium komen is onjuist.

A. K. Barua en A. Saran, Physica **29**, 1393, 1963.
H. F. P. Knaap en J. J. M. Beenakker, Physica, **27**, 523, 1961.

V

Bij het bepalen van de gevoeligheid van een ionisatiemeter met behulp van een geijkte MacLeod-manometer is gebruik van een koeler noodzakelijk. De systematische fout die hierbij optreedt wordt door Meinke en Reich verklaard met behulp van een mechanisme zoals in een kwikdiffusiepomp optreedt. Deze onderstelling is aanvechtbaar.

C. Meinke en G. Reich, Vakuum-Technik **12**, 79, 1963.

VI

Een Geiger-Müller-buis is voor ionendetectie in de massaspectrometrie minder geschikt dan men op grond van zijn grote gevoeligheid zou verwachten.

F. Kirchner en A. Benninghoven, Z. angew. Phys. **16**, 290, 1963.

VII

Georgian heeft een temperatuurschaal voorgesteld, waarbij de waarde van de universele gasconstante per definitie gelijk aan één wordt gesteld. Tegen deze temperatuurschaal zijn verschillende bezwaren aan te voeren.

J. C. Georgian, Nature **4920**, 695, 1964.

VIII

Metingen van kernspinroosterrelaxatietijden in supergeleidend aluminium van grote zuiverheid kunnen tot een te kleine waarde voor de energiespleet bij temperatuur nul leiden.

IX

Speciaal aan de hand van koorwerken kan men aantonen dat de muzikale waarden van de dodecafonie beslist niet berusten op de gelijkwaardigheid van de twaalf evenredig zwevende tonen in het octaaf.

X

Er zijn onvoldoende gronden om aan te nemen dat het mechanisme van de fotosynthese in purperbacteriën op twee primaire fotochemische processen, zoals voorgesteld door Clayton, is gebaseerd.

R. K. Clayton, Proc. Natl. Acad. Sci. U.S. **50**, 583, 1963.

XI

De wijze waarop O'Keeffe de stabilisatie van overgangsmetaalionen in gedeformeerde octaeders beschrijft is onvolledig.

M. O'Keeffe, J. Phys. Chem. Solids **21**, 172, 1961.

XII

Het verdient aanbeveling, dat bij studenten die in het genot zijn gesteld van een studiebeurs, alle studiekosten en andere kosten die uit het verkrijgen van de beurs voortvloeien als kosten van verwerving aftrekbaar worden gesteld voor de inkomstenbelasting.